Missouri S&T Library and Learning Resources

Scholars' Mine

Masters Theses

Student Theses and Dissertations

Summer 2014

Cervical cancer histology image feature extraction and classification

Peng Guo

Follow this and additional works at: https://scholarsmine.mst.edu/masters_theses

Part of the Bioimaging and Biomedical Optics Commons, Computer Sciences Commons, Electrical and Computer Engineering Commons, and the Radiology Commons

Department:

Recommended Citation

Guo, Peng, "Cervical cancer histology image feature extraction and classification" (2014). *Masters Theses*. 7302.
https://scholarsmine.mst.edu/masters_theses/7302

This thesis is brought to you by Scholars' Mine, a service of the Missouri S&T Library and Learning Resources. This work is protected by U. S. Copyright Law. Unauthorized use including reproduction for redistribution requires the permission of the copyright holder. For more information, please contact scholarsmine@mst.edu.

CERVICAL CANCER HISTOLOGY IMAGE FEATURE EXTRACTION AND CLASSIFICATION

by

PENG GUO

A THESIS

Presented to the Faculty of the Graduate School of the

MISSOURI UNIVERSITY OF SCIENCE AND TECHNOLOGY

In Partial Fulfillment of the Requirements for the Degree

MASTER OF SCIENCE IN ELECTRICAL ENGINEERING

2014

Approved by

R. Joe Stanley, Advisor
Randy H. Moss
William V. Stoecker

© 2014
PENG GUO
All Rights Reserved

ABSTRACT

Cervical cancer, the second most common cancer affecting women worldwide and the most common in developing countries can be cured if detected early and treated. Expert pathologists routinely visually examine histology slides for cervix tissue abnormality assessment. In previous research, an automated, localized, fusion-based approach was investigated for classifying squamous epithelium into Normal, CIN1, CIN2, and CIN3 grades of cervical intraepithelial neoplasia (CIN) based on image analysis of 62 digitized histology images obtained through the National Library of Medicine. In this research, CIN grade assessments from two pathologists are analyzed and are used to facilitate atypical cell concentration feature development from vertical segment partitions of the epithelium region for the same digitized histology images. Using features developed in this thesis with prior work, a particle swarm optimization and Receiver Operating Characteristic curve (ROC) explored for CIN classification showing exact grade labeling accuracy as high as 90%.

ACKNOWLEDGMENTS

First and foremost, I would like to express my sincere thanks to my advisor, Dr. R. Joe Stanley, for his kindly guidance, inspiration, and for the financial support he has provided throughout my research and studies. Dr. Stanley is the one who introduce me to the Digital Image Processing and Neural Network System field. He has always been encouraging me to seek the answer with considerable ideas and passion. I also wish to thank my committee members Dr. Randy H. Moss and Dr. William V. Stoecker for their great guidance and support.

I would like to thank all my friends and colleagues for sharing all the wonderful moments with me, sharing ideas with me and working with me. I would like to thank Cheng Lu, Koyel Banerjee and Xiao Pan for their company during those years, without the help of and cooperation of whose I couldn't have come up with so many new ideas and solved bunch of problems in research.

Finally, and most importantly, I am extremely grateful to my family, who have always wished the best for me and showered their great love and care on me. I would like to thank my mom for her most considerable support and love which gives me courage and faith to move on. And I couldn't forget the smile and delicious food from my cousin Jiahang Han and Aunt Changxin.

This research was supported by National Library of Medicine (NLM).

TABLE OF CONTENTS

Page

ABSTRACT iii

ACKNOWLEDGMENTS iv

LIST OF ILLUSTRATIONS vii

LIST OF TABLES ix

SECTION

1. INTRODUCTION 1

2. METHODOLOGY 3

3. MEDIAL AXIS DETECTION 5

4. NUCLEI AND LIGHT AREA DETECTION 9

4.1. NUCLEI PRE-PROCESSING 10

4.2 NUCLEI REGION SEGMENTATION (NUCLEI PROCESSING) 12

4.3 LIGHT AREA SEGMENTATION 14

5. FEATURE DEVELOPMENT 17

5.1 NUCLEI FEATURE DEVELOPMENT 17

5.2 LIGHT AREA FEATURE DEVELOPMENT 17

5.3 LAYER-BY-LAYER TRIANGLE FEATURES 18

5.4 COMBINED FEATURE DEVELOPMENT 23

6. CLASSIFICATION 30

6.1. CONTINUOUS CLASSIFICATION SCALE FOR DIFFERENT FEATURE COMBINATIONS COMPUTED FROM VERTICAL 30

6.2. EXPERIMENTS PERFORMED AND EXPERIMENTAL RESULTS ... 33

6.3. INTER-PATHOLOGIST IMAGE-BASED CLASSIFICATION OF DIGITIZED CERVICAL IMAGE DATA SET 37

7. ANALYSIS OF INTER-PATHOLOGIST EPITHELIUM CLASSIFICATION 43

7.1. THE CLASSIFICATION RESULTS IN BOTH EXPERTS AGREE WITH EACH OTHER ON WHOLE IMAGE CLASSIFICATION 44

7.1.1 Non-zero Existing in Any One of the 10 Segments 44

7.1.2 Zero Existing in Any One of the 10 Segments 65

7.2. THE CLASSIFICATION RESULTS IN WHICH TWO EXPERTS DISAGREE WITH EACH OTHER 72

8. CONCLUSION 80

BIBLIOGRAPHY 81

VITA 83

LIST OF ILLUSTRATIONS

Page

Figure 1.1. CIN grading label examples 1

Figure 2.1. Overview of CIN grade classification method developed in this study. 3

Figure 3.1. Examples of improper medial axis estimation. 5

Figure 3.2. New medial detection 6

Figure 3.3. Example of medial axis found using bounding box-based algorithm.. 7

Figure 4.1. Original large image with green boundary. 9

Figure 4.2. Dividing the original image into sub-images of 10 and 5.. 10

Figure 4.3. Original image and edge detector images. 11

Figure 4.4. Method of image sharpening 11

Figure 4.5. Images and histograms before and after Histogram-Equalization. 12

Figure 4.6. Nuclei detection progress 13

Figure 4.7. Result images in three different color channels. 14

Figure 4.8. Original epithelium and the light area segmentation. 16

Figure 5.1. Progress of locating nuclei (vertex) in three different layers. 19

Figure 5.2. Distribution of triangles for the entire image. 20

Figure 5.3. Distribution of triangles in a single image. 22

Figure 7.1. Single segments which are given "0". 66

Figure 7.2. Whole image examples..... 74

Figure 7.3. Distribution of different CIN grading scales over 620 segments.... 77

Figure 7.4. Distribution of individual segment classifications which match the whole image CIN classifications. 78

Figure 7.5. Distribution of individual segment classifications which match the whole image classifications where there is variation in the 10 individual segments within an image..... 78

Figure 7.6. Distribution of segment results which match the final classification results (without all same results, and group with 2 different CIN levels). 79

LIST OF TABLES

Page

Table 5.1. Feature table..... 23

Table 6.1. Input variables for each single segment among 10 vertical segments..... 32

Table 6.2. Input variables for each single segment among 5 vertical segments..... 33

Table 6.3. Image-based classification results using PSO neural network approach for continuous classification scale..... 34

Table 6.4. Classification results for 5segments with different feature combinations using Exact Class Label, Off-by-One Window, Normal vs. CIN, and Normal vs. CIN1 vs. CIN2 or CIN3..... 36

Table 6.5. Classification results for different feature combinations based on 10 vertical segments using Exact Class Label, Off-by-One Window, Normal vs. CIN, and Normal vs. CIN1 vs. CIN2/CIN3..... 37

Table 6.6. Classification results based on CIN truth grades from Dr. Frazier for different feature combinations based on 10 vertical segments using Exact Class Label, Off-by-One Window, Normal vs. CIN, and Normal vs. CIN1 vs. CIN2/CIN3. 38

Table 6.7. Classification results for different feature combinations with 10 vertical segments for Exact Class Label, Normal vs. CIN, and CIN1 vs. CIN2/CIN3 based on Dr. Frazier's CIN labeling..... 39

Table 6.8. Classification results for different feature combinations with 5 vertical segments for Exact Class Label, Normal vs. CIN, and CIN1 vs. CIN2/CIN3 based on Dr. Frazier's CIN labeling..... 41

Table 7.1. Both experts agree on whole image and individual segment normal grade classification (11 images total). 45

Table 7.2. Experts both agree on CIN 1 grades for whole image and all segments have CIN 2 grades (5 images total).. 50

Table 7.3. Experts both agree on CIN 2 labels on whole image and individual segment grades (4 images total). 52

Table 7.4. Experts both agree on CIN 3 labels on whole image and individual segment grades (3 images total). 54

Table 7.5. Whole image and individual segment CIN classifications for 15 images where both experts agree on the whole image classification and the individual segment classifications vary from the whole image. 56

Table 7.6. Whole image and individual segment CIN classifications for 9 images where both experts agree on the whole image classification and the individual segment classifications vary from the whole image. 62

Table 7.7. Whole image and individual segment CIN classifications for 4 images where both experts agree on the whole image classification with an inconclusive individual segment classification (“0”). 66

Table 7.8. Whole image and individual segment CIN classifications for 4 images where both experts agree on the whole image classification with an inconclusive individual segment classification (“0”). 68

Table 7.9. Image example with end segments as inconclusive (“0”) where both experts agree on the whole image classification..... 71

Table 7.10. Whole image CIN classifications on which the experts disagree with each other. 72

Table 7.11. Whole image classification examples in which experts disagree and with multiple results within 10 segments 75

1. INTRODUCTION

Annually, there are 400,000 new cases of invasive cervical cancer out of which 15,000 occur in the U.S. alone [1]. Diagnosis for cervix tissue abnormalities is commonly performed procedures, including Pap test, a colposcopy to visually inspect the cervix, and visual inspection of histology slides when biopsied cervix tissue is available Expert pathologist visual inspection of histology slides has been used as a standard of diagnosis [2]. Pathologists commonly assess Cervical Intraepithelial Neoplasia (CIN), provide diagnoses related to CIN and its various grades based on the visual interpretation of histology slides [3–7]. As part of the pathologist diagnostic process, Cervical intraepithelial neoplasia (CIN) is a pre-malignant condition for cervical cancer in which the atypical cells are examined in the epithelium [3] and is commonly assessed in the visual inspection of histology slides [3,7]. As shown in Figure 1.1, Cervical biopsy diagnoses include Normal (that is, no CIN lesion), and three grades of CIN, CIN1, CIN2 and CIN3 [3–5]. CIN1 corresponds to mild dysplasia (abnormal change), while CIN2 and CIN3 are used to denote moderate dysplasia and severe dysplasia, respectively.

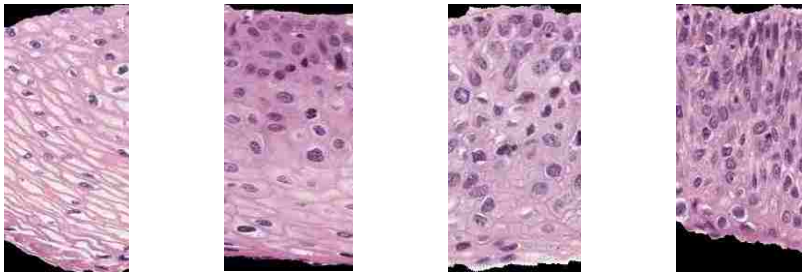

Figure 1.1. CIN grading label examples. (a) Normal, (b) CIN 1, (c) CIN 2, (d) CIN 3.

In previous research, the research group investigated cervix histology image analysis techniques using a localized, fusion-based approach to classify the epithelium region into the different CIN grades, as determined by an expert pathologist [8]. There were 66 features presented including texture, color, triangle, WDD features which yield an exact classification result of 70.5% [8].

The remainder of this thesis is organized as follows. Section 2 presents the methodology of the research. Section 3 is about the algorithms for medial axis detection and details on vertical segmentations. Section 4 presents details about nuclei and light area detection and segmentation. Section 5 gives explanations of feature groups which include the nuclei, combined and layer-by-layer triangle features. Section 6 presents the neural network used in classification in this research and the experimental results yielded which is completed by Dr. Stanley and Koyel Banerjee. Section 7 presents my CIN classification analysis of two pathologists including comparison and detail analysis between all the classification results. Section 8 presents the conclusion of the thesis. My unique contributions in this research are: 1) the development of nuclei and light area detection and segmentation (Section 4), 2) the development of nuclei, combined, layer-by-layer triangle features (Section 5) and 3) the analysis of inter-pathologist epithelium classification (Section 7).

2. METHODOLOGY

The goal of this research is to classify the squamous epithelium regions from cervix histology images into different grades of CIN. In the research, 62 cervix histology images were obtained in collaboration with the National Library of Medicine (NLM), with the epithelium manually segmented and CIN grade classifications determined by an expert pathologist. The research presented in this thesis extends the study in [8] for the development of new image analysis and classification of individual vertical segments for whole image for CIN grade determination. Figure 2.1 shows the flowchart of the overall method developed in this study for CIN grade classification. This thesis also presents CIN grade comparative classification analysis for two expert pathologist CIN grading of the 62 image data set.

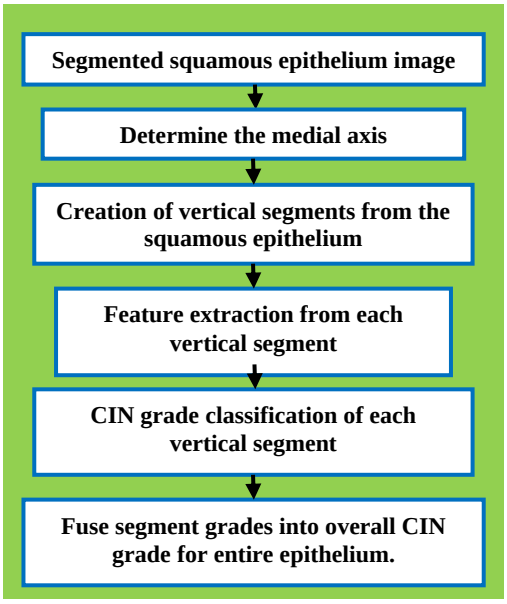

Figure 2.1. Overview of CIN grade classification method developed in this study.

Figure 2.1 before can be concluded as several steps followed:

- Medial axis detection, locate the medial axis of the segmented epithelium region which is mainly finished by Soumya De and Koyel Banerjee;
- Image segmentation, divide the segmented image into 5 or 10 different vertical blocks along the medial axis by Soumya De.
- Feature extraction, extract features from each of the blocks in which is done by me with creating and testing several feature groups that help a lot in classification.
- Image Classification, classify each of these segmented blocks into the different CIN cervical cancer grades in which is developed by Dr. Stanley and Koyel Banerjee.

3. MEDIAL AXIS DETECTION

The medial axis determination algorithm is presented here as one of the steps for epithelium analysis for CIN grade classification. This approach for medial axis detection was developed by Koyel Banerjee and Soumya De [12]. The approach used to involve distance transform to estimate the interior 60% of the medial axis with the bounding box of the epithelium region to project the distance transform-based medial axis to the median bounding box points for the left- and right-hand end points (remaining left-hand 20% and right-hand 20% portions of the axis) [8,9]. However, the algorithm had difficulties finding the left- and right-hand portions of the axis in histology images with a somewhat rectangular epithelium region. Figure 3.1 shows three examples of improper medial axis estimation using the distance transform-based approach. The line shown in pink color is the detected medial axis using the distance transform approach while the line shown in green is the manually marked medial axis, which is the desirable medial axis. In order to address these limitations with medial axis determination, a bounding box-based method was explored.

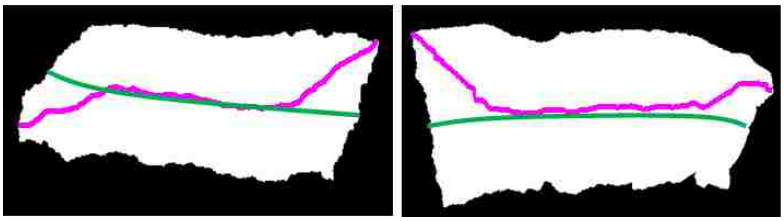

Figure 3.1. Examples of improper medial axis estimation.

The bounding box-based medial axis estimation algorithm (new approach) is a two steps method. One of the methods follow the original method by using the distance transform and then finding out the centroid points at the end segments for correction along the end segments and prevent bending or deflection of the medial axis along the edges. The second and new approach however uses the morphology of the epithelium area under consideration before making the decision about which method to follow for the axis detection.

The bounding box-based method is mainly based on ratio comparison of the number of nuclei distributed over 8 masks that are created from the bounding box and control points marked on it. Also for precision purposes a 16 mask approach along with symmetry factor of the image was taken into consideration. The following Figure 3.2 explains the concept.

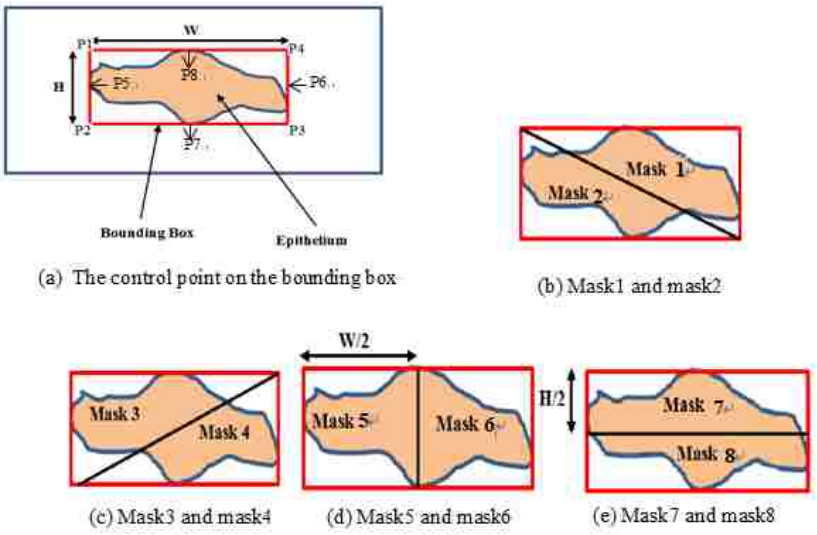

Figure 3.2. New medial detection.

The masks are used to help in computing the ratios of the number of detected nuclei to the ratio of the area of the masks. For example if the number of nuclei in mask 1 in Figure 3.2 is supposed to be n1 and I mask 2 is n2 then Koyel Banerjee compute a ratio as f1=n1/n2 . She also computes another set of ratios as $\frac{n_1}{f_1}$and $\frac{n_2}{f_1}$ for normalizing the n (n_1, n_2..) values. Finally she multiplied this result by the eccentricity value of the particular mask . The equation guiding the detection of the medial axis can be given asv $= \frac{n \times f}{e}$ where n symbolizes the array containing the normalized ratios of $n_1, n_2,$ $n_3 \ldots . n_8$, f symbolises the array containing $f_1,\ f_2 \ldots . f_8$ and e contains the eccentricity measures of all the eight masks and e represents the eccentricity value of the entire tissue slide. The idea is that whichever position gives the maximum value by this computation is the medial axis position. Position 1 and 2 gives the medial axis as shown in Figure 3.3 and so on, respectively. Some of the medial axis image examples are stated below.

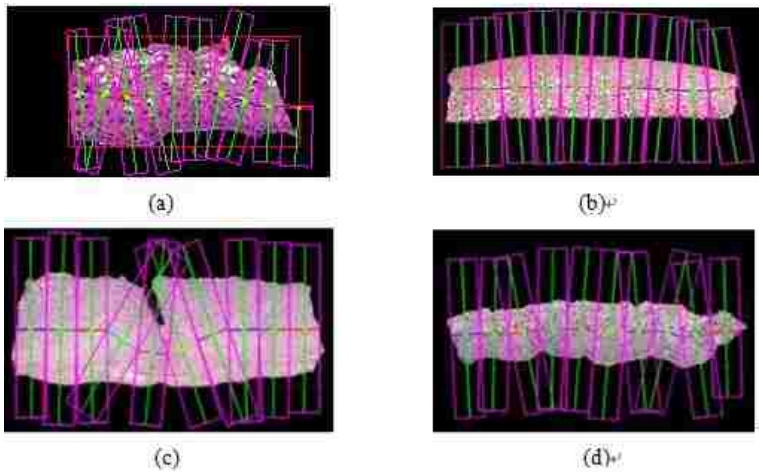

Figure 3.3. Example of medial axis found using bounding box-based algorithm. (a) And (b) show bounding box method with axis extending beyond epithelium region. (c) And (d) show bounding box updated algorithm with medial axis contained with epithelium region.

As seen from the right-hand medial axis example image in Figure 3.3, some of the segments extend way out of the actual epithilial region. This is because in this approach points on the bounding box which is exterior to the epithilium region was used. However, for such cases during feature extraction the code outputs zero as output meaning that no epithilium region was under consideration under those vetical segemented parts. Later on the classification preocess discards such segments and take up only valid segments out of the ten segments for an image for decision of CIN label.

4. NUCLEI AND LIGHT AREA DETECTION

The nuclei and light area detection method is presented here as an important step for feature extraction and further for classification, which is developed by Cheng Lu and myself. The algorithm can extract nuclei area and light area out of the whole epithelium region. As what is found, each given image contains two separate files, one in jpg format and the other in XML format. The jpg format is the visual representation of the sample. The Extensible Markup Language (XML) file is a format that is both human-readable and machine-readable. The XML file marks the boundary position for the jpg image. The boundary position differentiates the useful area and outside area. As shown in Figure 4.1, the light area above the green box is not considered in the region of interest, since it is not a part of the squamous epithelium.

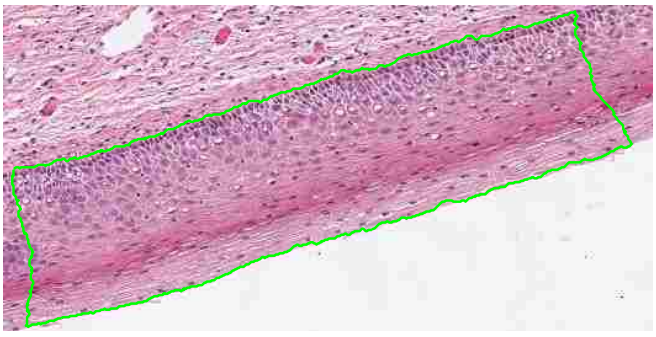

Figure 4.1. Original large image with green boundary.

Previous research has explored dividing the ROI into 10 vertical segments (sub-images) along the uniform points along the medial axis [8]. First, to definite the

vertical segments are determined, a big bounding box which contain the whole epithelium is created with the help of medial axis; then, the box is divided in parts respecting to the medial axis, each of which is the single segment among the total 5 or 10.

Current research is examining 5 vertical segments for epithelium region analysis and classification. In continuation, a data set of 620 sub-images (10 vertical segments from each of the 62 images) from the original 62 images is created which were obtained from the National Library of Medicine (NLM). The following Figure 4.2 shows some samples of sub-images.

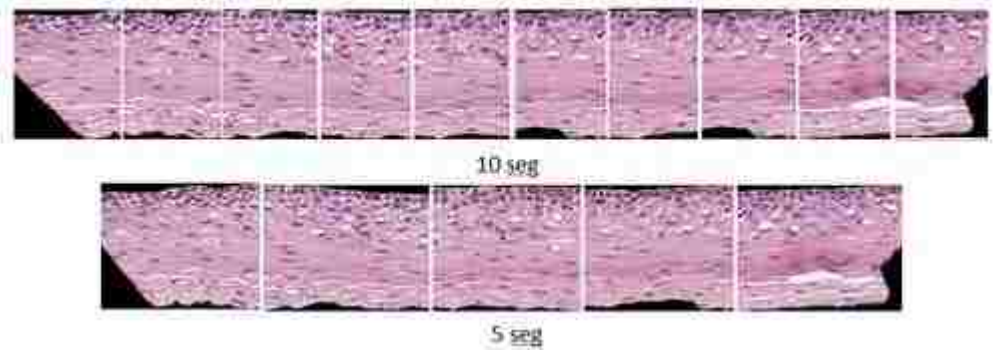

Figure 4.2. Dividing the original image into sub-images of 10 and 5.

4.1. NUCLEI PRE-PROCESSING

A second new feature in this study was the investigation of a nuclei detection algorithm based on epithelium image pre-processing to make the image enhanced for nuclei detection. These pre-processing procedures include averaging, image sharpening, histogram-equalization, high frequency boosting, etc.

There are two steps in this segmentation process, image enhancement and nuclei detection. Before nuclei detection, I take a step of image enhancement of the gray scale image. There are many different approaches for image enhancement. For this project, a variety of filters are applied to the images, including Laplacian, Canny, Roberts and Sobel as shown in Figure 4.3.

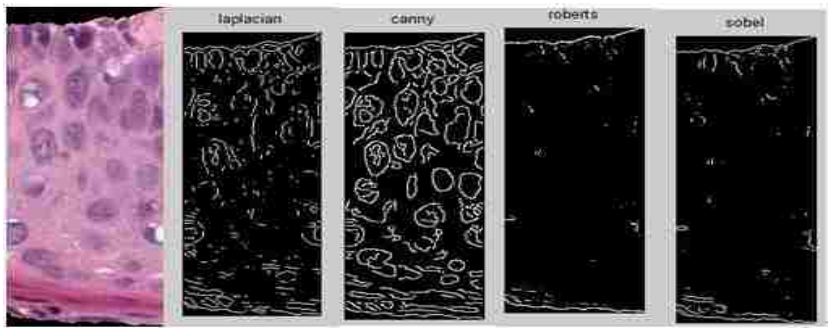

Figure 4.3. Original image and edge detector images.

An image enhancement process called High-boost Filtering is used to improve the contrast between the nuclei and the background which is shown in Figure 4.4.

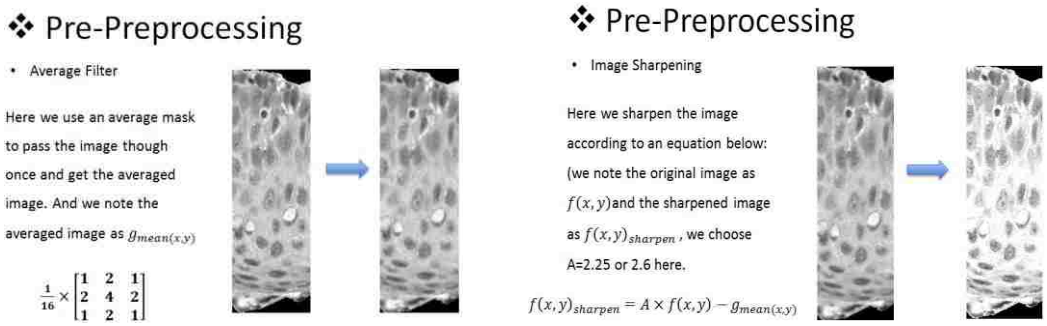

Figure 4.4. Method of image sharpening.

$$I_{sharpen}(x, y) = A * f(x, y) - g(x, y)$$

From the equation and Figure 4.4 before, f (x, y) is the original image. "$g(x, y)$" is calculated from passing an averaging filter to the original image. A is varied by the result from the output image. After optimization, a value of 2.25 is used as "A". The "$I_{sharpen}(x, y)$" is the resulting image as shown in Figure 4.5. After using High-boost filter, histogram equalization is applied to the image. This step equalizes the values in each pixel, so the range of values is equally distributed from 0 to 255 as shown in Figure 4.5.

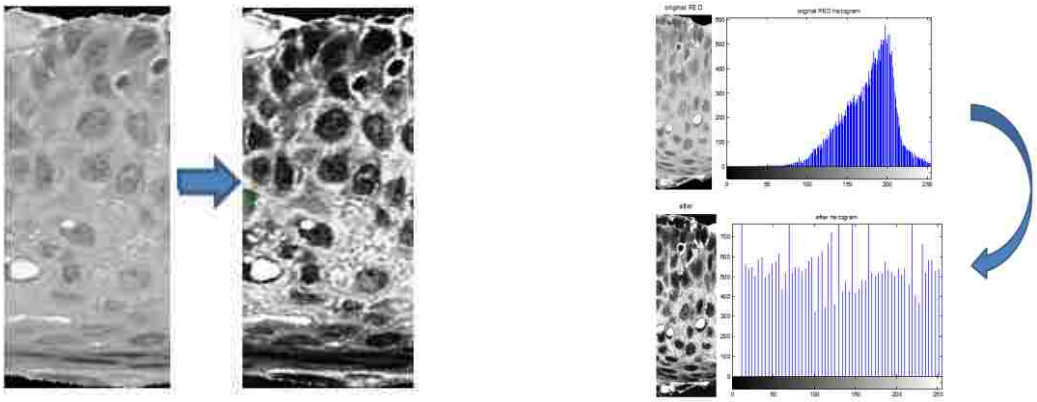

Figure 4.5. Images and histograms before and after Histogram-Equalization.

4.2 NUCLEI REGION SEGMENTATION (NUCLEI PROCESSING)

After testing and correction, Cheng Lu and I use a portion of the nuclei detection code which was supplied by NLM and it has many progresses such as clustering, holes filling, thresholding, etc, which is shown in Figure 4.6.

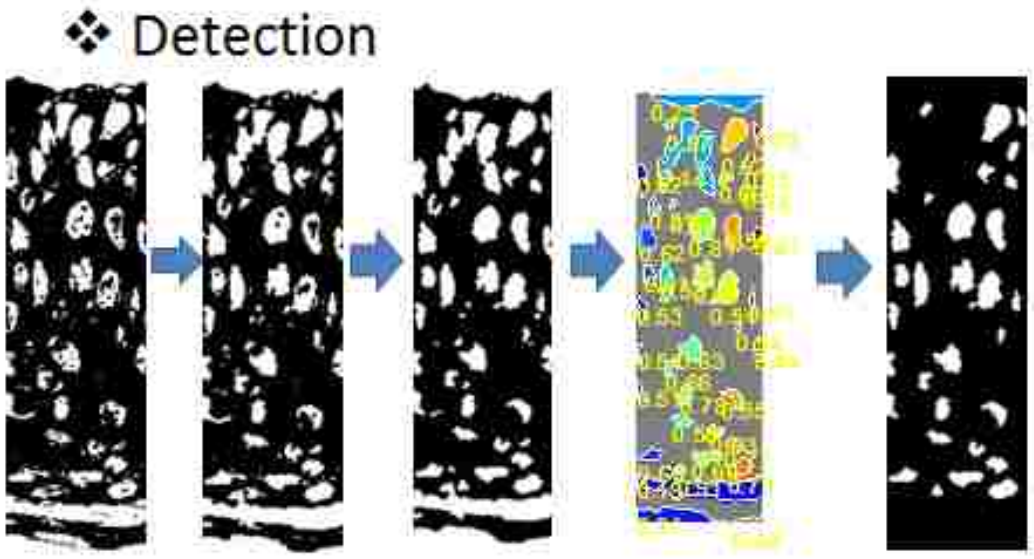

Figure 4.6. Nuclei detection progress.

At the very beginning of all the procedures, K-means clusters are taken from the image after the former steps of pre-processing [10]. Since the contrast of the images is improved, the nuclei detection code can produce a better result. The initial plan for this project is only processing the red layer of the RGB image. After examination, the green and blue layers give similar but slight different resulting images as shown in Figure 4.7. Even though three layers have very similar result, but none of them gives a conclusive result. It is possible to have a better result by combining all three layers, but time consuming is the only disadvantage for this approach. It takes three times more calculation time to process three layers instead of one. After careful consideration a decision is made that only process red layer and take the consequence of losing some of the small region.

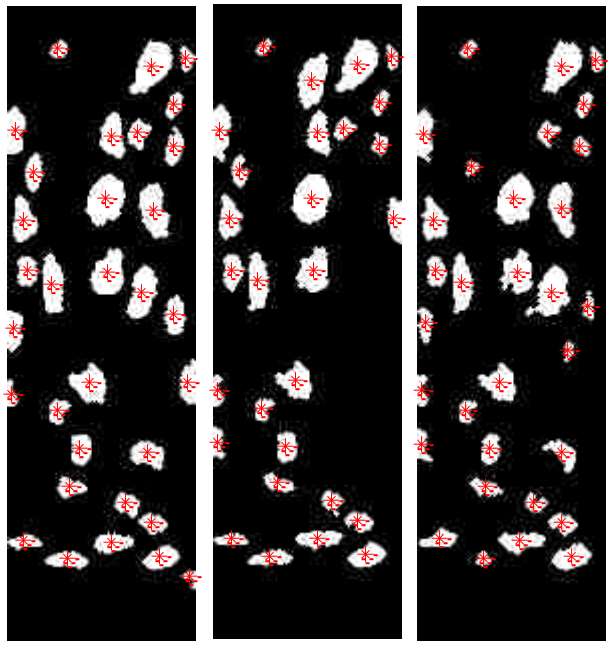

Figure 4.7. Result images in three different color channels. (a) Red layer, (b) green layer, (c) blue layer.

4.3 LIGHT AREA SEGMENTATION

With the help of the nuclei detection results, light area segmentation can be achieved with a good result. The algorithm is developed by Xiao Pan and Koyel Banerjee involving the nuclei detection results from Cheng Lu and me. The challenge that goes with extracting the light area regions from the original image is mainly the color and intensity variations. Often the light areas are mistaken for white areas which are not the case. The light areas may appear white to the human eye, but the light areas tend to be more on the tail on the histogram where there is the concentration of light areas or high intensity values. Also the other problem faced was that the light areas do not have a pre-defined shape like the nuclei so it cannot be taken into account the shape/morphology of these regions. Therefore, to avoid such shortcomings an attempt to process these

regions in the color plane was done taking into account the a-plane and b-plane and discarding the L-plane. The L-plane provided the best visual results of the 3 planes examined.

The following outlines the methods undertaken to segment the histology images:

1. Conversion from RGB color space to L*a*b color space and taking out the luminance components that is the L plane for working further on it.

2. Adaptive histogram equalization is performed on the image from step 1 as an alternative to using ‘histeq’. While ‘histeq’ works on the entire image, ‘adapthisteq’ operates on small regions in the image, called tiles. Each tile's contrast is enhanced, so that the histogram of the output region approximately matches a specified histogram. After performing the equalization, ‘adapthisteq’ combines neighboring tiles using bilinear interpolation to eliminate artificially induced boundaries.

3. After the image has been sufficiently contrast adjusted so that the light areas appear lighter and the dark areas appear darker for facilitating the extraction, thresholding is performed with a value of 0.6 as obtained by trial and error analysis. This step generally gets rid of the very dark nuclei regions leaving behind the lighter nuclei and epithelium along with the light areas.

4. Finally, to segment out the light areas, Koyel and I perform a general classification step using the K-means algorithm. K-means clustering is a method of cluster analysis which aims to partition n observations into k clusters in which each observation belongs to the cluster with the nearest mean. This results in a partitioning of the data space into Voronoi cells. This is crucial for segmenting the light areas since these areas do not have a fixed color value neither do they have a fixed contour or shape. Koyel

and I cluster the image into 4 observations and work further on with the cluster giving the value for the lighter most regions in the epithelium.

5. After the final cluster of importance has been obtained to get rid of the finer connected light regions, a morphological dilation is presented followed by erosion with "disk" as structure element and 2 as radius. Then, "regionprops" is performed on the remaining image objects to keep only those light areas which are greater than an area of 100 pixels.

The resulting large light areas are used for feature calculations for epithelium vertical and image-based classification which are shown in Figure 4.8.

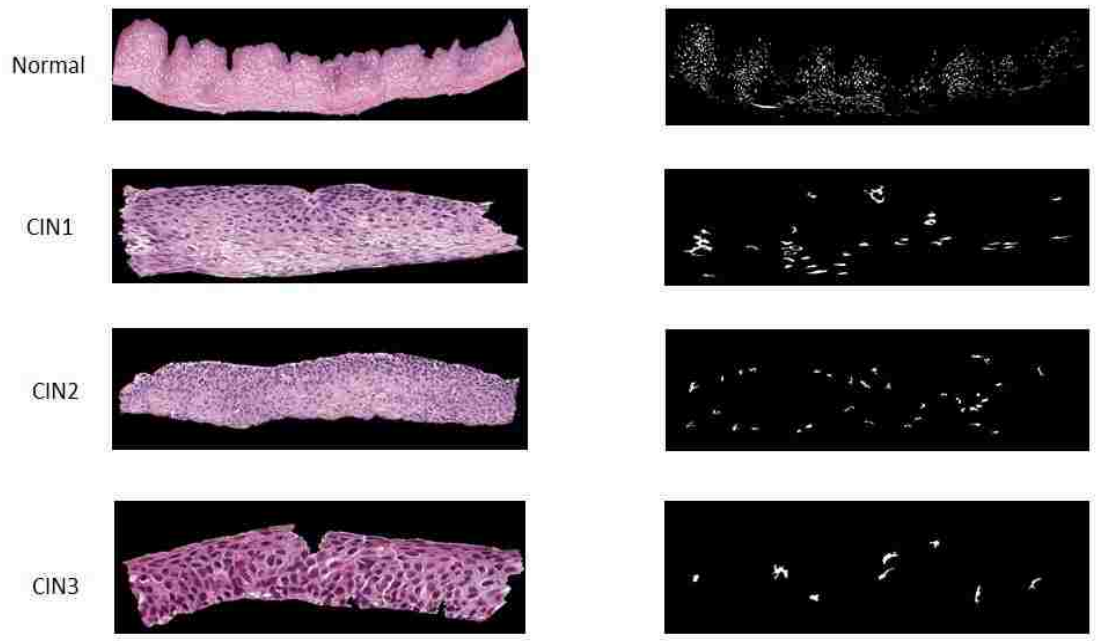

Figure 4.8. Original epithelium and the light area segmentation.

5. FEATURE DEVELOPMENT

5.1 NUCLEI FEATURE DEVELOPMENT

Nuclei feature development are presented here as a very important feature, which gives the situation of the nuclei on the epithelium region that related to the classification of CIN stage. The algorithm is developed by Cheng Lu [11] and myself, including two features calculated within vertical segments as shown below:

1. Number of nuclei

2. Nuclei area over background area

The steps for computing the nuclei-based features are as follows. First, with the nuclei detected, in an image called nuclei mask, the number of nuclei can be counted, also the nuclei area can be found.

Second, the region of epithelium background with the help of nuclei mask is got, and the area of background is calculated. Then, compute the ratio.

5.2 LIGHT AREA FEATURE DEVELOPMENT

For each vertical segment within the epithelium, to define the classification by light areas, Xiao Pan and Koyel obtain some relative feature data. They are ratio RGB, ratio R, ratio G, ratio B, ratio of luminance image in L plane, number of light area in per area and the ratio of light area to background area separately. The exact procedures are as follow:

1. Obtaining the mask of light area, RGB segmented image and luminance image.

2. Calculating the average intensity of the RGB segmented image and the associated average background intensities.

3. The same algorithm to get the average intensity of R-plane, G-plane, B-plane, L-plane in luminance image and the associated average background intensities backgrounds.

4. Obtain the total number and final areas of white parts, and calculate the total area of the whole image.

5. Dividing the average intensity of RGB image by its background area which is the area except white area to obtain the ratio of RGB.

6. The same calculation to get ratio of R, ratio of G, ratio of B, ratio of luminance.

7. Dividing the total number of white parts by total area of the whole image to get the number of white area in per unit area.

8. Compute the ratio of light areas to background areas.

5.3 LAYER-BY-LAYER TRIANGLE FEATURES

The layer-by-layer triangle algorithm and the features generated are presented here, which are developed by me, taking advantages the concept of “Delaunay Triangle” [13]. In this algorithm, the nuclei detection result is imported to locate the position of the nuclei which are used as vertices forming the Delaunay triangles. In the previous research [8], triangle features are developed according to the whole segment and the way to locate nuclei (vertices) is Hough-transform included in the triangle function. The features that are obtained from the triangles include: average area of the triangles, standard deviation

of the area of the triangles, average distance between the vertices of the triangles found and standard deviation of the distance between the vertices of the triangles.

Most of the features are obtained with respect to the nuclei detection results which make it more accurate. And each vertex is the centroid of every nuclei detected. Also, the whole epithelium is no longer the focus but the three different layers generated after dividing a single segment horizontally into 3 parts. The reason for this is that the situation of each layer is changing and has some characteristic features when it is in different CIN stage, which can be taken advantage of making a proper diagnosis. Processing the nuclei detection result is shown in Figure 5.1, where the circles in three colors mark the centroids of nuclei in three different layers.

Also, the triangle algorithm is re-coded by importing nuclei detection results instead of using Hough-transform to locate the nuclei (vertices), the features that are obtained are shown from F96-F100 in the feature sheet.

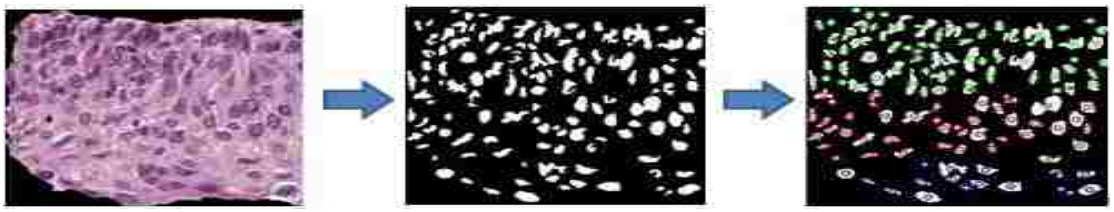

Figure 5.1. Progress of locating nuclei (vertex) in three different layers.

Then, Delaunay triangles can be figured out as what is shown in Figure 5.2, and what need to be informed is that this is the Delaunay triangles based on all the nuclei of

one piece of vertical segment among 5 or 10 totally, which is different from the algorithm here to be presented, where a single segment is processed in three parts (or three layers horizontally).

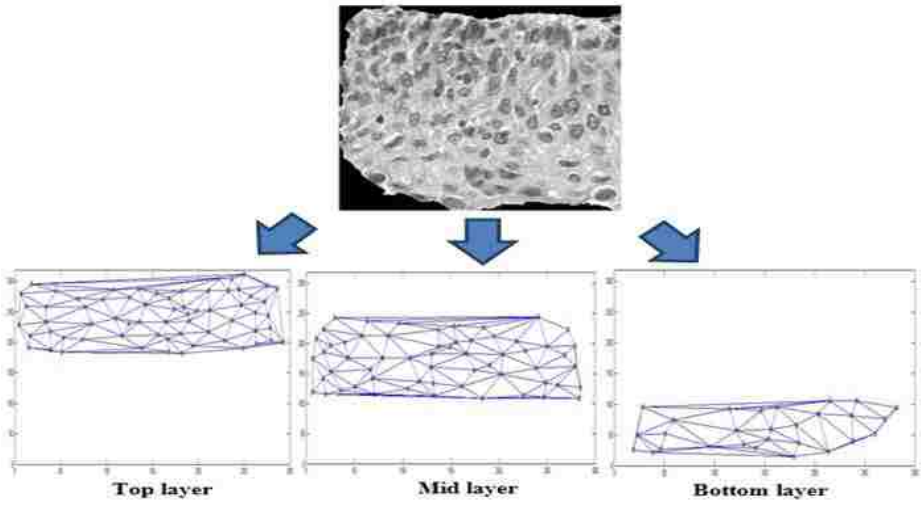

Figure 5.2. Distribution of triangles for the entire image.

The top/bottom orientation of the epithelium is determined so that the higher density level of nuclei is top and the lower density is bottom, so that all the features obtained from calculation can be in a same order, which makes them useful and comparable. For one certain image, size known, higher density goes with the number of nuclei in a certain area, which leads to the method of determining the top. After equally dividing the whole image by parts in a horizontal direction, the one contains the largest number of nuclei should be the top part.

The next step is to divide the whole epithelium in three layers, as the edges of bounding box are very closed to the boundary of the epithelium, it can be used to divide the whole epithelium into 3 different parts as wanted: upper-layer, which is the top 1/3 of the whole bounding box, the mid-layer which is the middle 1/3 and the lower layer which is the bottom 1/3. The distribution of triangles for three different layers in Matlab is shown in Figure 5.2.

Then, different features are calculated based on three different layers, the number of triangles in each layer, average area of the triangles in each layer, average edge distance of triangles in each layer, and the standard deviation of the two former features. For these triangle features mentioned, which describe different aspects of CIN stages, are all generalized by dividing the square root of epithelium area in the single vertical segment. The number of triangles can be another way of showing the number of nuclei existing per unit area, and it could be evidence of current CIN stage since the higher the CIN stage goes, relatively more nuclei would be there in per unit area of epithelium region. And the same thing happens on the average area of the triangles which shows the number of triangles existing per unit area of epithelium region. Also the information of nuclei density is reflected on the feature value of average edge distance and standard deviation of triangles, as the longer the average edge distance be, the lower density would be.

Figure 5.3 presents an example image where the lines represent the edges of the triangles and the vertices represent the positions of nuclei found and the different colors show the different layers.

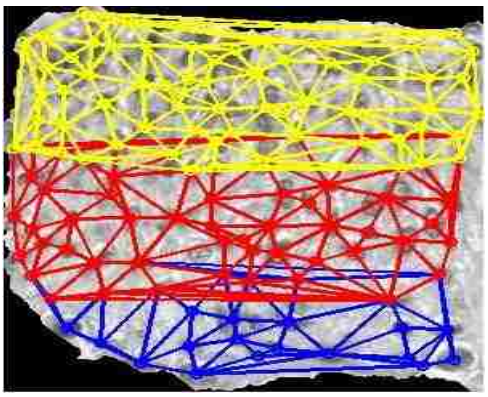

Figure 5.3. Distribution of triangles in a single image.

Where attention needed to be paid is the small overlaps between different layers, which come from the method used to locate the top or bottom point of each layer. In this algorithm, nuclei itself is used with the bounding box coordinate system to locate the lowest or the highest point. The reason is that if only the coordinate system is used to sharply cut the whole epithelium vertically by 3 parts, some of the nuclei would also be cut in parts, resulting in lack of nuclei in certain layer to form a single triangle, which would have given worse result and affect the counting of triangles and nuclei. As a result, nuclei are also involved in locating the boundary of different layers to which the judging point lies where the nearest position in which a complete nuclei can be figured out, one pixel off. Note that a similar process is process for Triangle feature calculations and analysis for both 5 and 10 vertical segments.

5.4 COMBINED FEATURE DEVELOPMENT

Combined feature is a feature group Cheng Lu [11] and I developed to indicate the condition of CIN stage with respect to both nuclei and light area features. Table 5.1 below presents features investigated in this thesis and previous research [8] (Texture Features, Color Features, Triangle Features, and Correlation-based Features and the features currently under development (Nuclei Features, Light Area Features, and Combined Features), summarized as follows.

After both the nuclei features and the light area features were extracted, some new features were generated by using some of the new attributes from nuclei and light area features. Such features include the ratio between the number of light areas and the number of nuclei, and the ratio between total light areas and total nuclei areas.

Table 5.1. Feature table,(a) texture, (b) color, (c) triangle, (d) WDD, (e) nuclei, (f) light area, (g) combined, (h, i, j, k, l) layer-by-layer triangle

Feature Set	Label	Measure	Description
(a) Texture Features	F1	Contrast of segment	Returns a measure of the intensity contrast between a pixel and its neighbor over the whole image.
	F2	Energy of segment	Measures the entropy (sum of squares of pixel values in the segment)
	F3	Correlation of segment	Returns a measure of how correlated a pixel is to its neighbor over the whole image.
	F4	Homogeneity of a segment	Returns a value that measures the closeness of the distribution of pixels in the segment to the segment.

Table 5.1. Feature table,(a) texture, (b) color, (c) triangle, (d) WDD, (e) nuclei, (f) light area, (g) combined, (h, i, j, k, l) layer-by-layer triangle (Cont.)

	F5-F6	Contrast of GLCM	Measure of the contrast of the GLCM matrix obtained from the segment.
	F7-F8	Correlation of GLCM	Returns a value that measures the closeness of the distribution of elements in the GLCM to the GLCM diagonal.
	F9-F10	Energy of GLCM	Returns the sum of squared elements in the GLCM.
	F11	Correlation of GLCM	Returns a value that measures the closeness of the distribution of elements in the GLCM to the GLCM diagonal.
(b) Color Features	F12	Percentage Red	Percentage of region that has the reddish pixels.
	F13	Percentage White	Percentage of region that has the whitish pixels.
	F14	Percentage Black	Percentage of region that has the blackish pixels.
(c) Triangle Features	F15	Average area of triangles	This is the average area of the triangles formed by using Delaunay triangulation on the cells detected.
	F16	Std deviation of area of the triangles	This is the standard deviation of the area of the triangles formed by using Delaunay triangulation on the cells detected.
	F17	Average edge length	This is the mean of the length of the edges of the triangles formed.
	F18	Std deviation of edge length	Standard deviation of the length of the edges of the triangles formed.

Table 5.1. Feature table,(a) texture, (b) color, (c) triangle, (d) WDD, (e) nuclei, (f) light area, (g) combined, (h, i, j, k, l) layer-by-layer triangle (Cont.)

(d) Correlation -based Features (WDD Features)	F19~F66	Weighted density distribution	Correlation of texture profile of the segment and WDD function.
(e) Nuclei Features	F67	Average nuclei area	Returns the ratio of total nuclei area over total number of nuclei
	F68	Ratio of background area over nuclei area	Returns the ratio of total background (Nuclei) area over total nuclei area
(f) Light Area Features	F69	Ratio RGB	Returns the average intensity of RGB image over background
	F70	Ratio R	Returns the average intensity of R-plane in luminance image over background
	F71	Ratio G	Returns the average intensity of G-plane in luminance image over background
	F72	Ratio B	Returns the average intensity of B-plane in luminance image over background
	F73	Ratio LUM	Returns the average intensity of L-plane in luminance image over background
	F74	Unit size of light area	Returns the number of light area over total area
	F75	Ratio of light area over background area	Returns the ratio of total light areas over total background (Light) area
(g) Combined Features	F76	Light area number over nuclei number	The ratio of light area number over nuclei number
	F77	Ratio Light over Nuclei	The ratio of total light areas over total nuclei area

Table 5.1. Feature table,(a) texture, (b) color, (c) triangle, (d) WDD, (e) nuclei, (f) light area, (g) combined, (h, i, j, k, l) layer-by-layer triangle (Cont.)

(h) Triangle Features (Vertices detected with the original algorithm of F15-F18)	F78-F80	Average area of triangles In upper, mid and lower layer	This is the average area of the triangles formed by using Delaunay triangulation on the cells detected, from the upper layer to the lower layer.
	F81-F83	Std deviation of area of the triangles in upper mid and lower layer	This is the standard deviation of the area of the triangles formed by using Delaunay triangulation on the cells detected, from the upper layer to the lower layer.
	F84-F86	Average edge length of the triangles in upper mid and lower layer	This is the mean of the length of the edges of the triangles formed, from the upper layer to the lower layer.
	F87-F89	Std deviation of edge length of triangles in upper mid and lower layer	Standard deviation of the length of the edges of the triangles formed, from the upper layer to the lower layer.
	F90-F92	Number of triangles in three layers divided by square root of epithelium area	Counting the number of triangles in three different layers
	F93-F95	Number of triangles	The ratio of number of triangles over the area of the three different layers and the total triangle number over the total area in the last feature
(i) Triangle Features (Vertices detected as Nuclei centroids but not in three layers)	F96	Average area of triangles In upper, mid and lower layer	This is the average area of the triangles formed by using Delaunay triangulation on the cells detected, from the upper layer to the lower layer.

Table 5.1. Feature table,(a) texture, (b) color, (c) triangle, (d) WDD, (e) nuclei, (f) light area, (g) combined, (h, i, j, k, l) layer-by-layer triangle (Cont.)

(j) Triangle Features (Vertices detected as Nuclei centroids but not in three layers)	F97	Std deviation of area of the triangles in upper mid and lower layer	This is the standard deviation of the area of the triangles formed by using Delaunay triangulation on the cells detected, from the upper layer to the lower layer.
	F98	Average edge length of the triangles in upper mid and lower layer	This is the mean of the length of the edges of the triangles formed, from the upper layer to the lower layer.
	F99	Std deviation of edge length of triangles in upper mid and lower layer	Standard deviation of the length of the edges of the triangles formed, from the upper layer to the lower layer.
	F100	Number of triangles in three layers divided by square root of epithelium area	Counting the number of triangles in three different layers
	F101	Number of triangles	The ratio of number of triangles over the area of the three different layers and the total triangle number over the total area in the last feature
(k) Layer-by-layer Triangle Features	F102-F104	Average area of triangles In upper, mid and lower layer	This is the average area of the triangles formed by using Delaunay triangulation on the cells detected, from the upper layer to the lower layer.
	F105-F107	Std deviation of area of the triangles in upper mid and lower layer	This is the standard deviation of the area of the triangles formed by using Delaunay triangulation on the cells detected, from the upper layer to the lower layer.

Table 5.1. Feature table,(a) texture, (b) color, (c) triangle, (d) WDD, (e) nuclei, (f) light area, (g) combined, (h, i, j, k, l) layer-by-layer triangle (Cont.)

(k) Layer-by-layer Triangle Features	F108-F110	Average edge length of the triangles in upper mid and lower layer	This is the mean of the length of the edges of the triangles formed, from the upper layer to the lower layer.
	F111-F113	Std deviation of edge length of triangles in upper mid and lower layer	Standard deviation of the length of the edges of the triangles formed, from the upper layer to the lower layer.
	F114-F116	Number of triangles in three layers	Counting the number of triangles in three different layers
	F117-F119	Number of triangles over area of the layer	The ratio of number of triangles over the area of the three different layers and the total triangle number over the total area in the last feature
	F120	Total number of triangles over total area	The ratio of number of triangles over the area of the whole epithelium
	F121	Background area over total triangle area	The ratio of background area over the area of all the triangles
(l) Triangle Features (Vertices as centroids but with original methods of feature F15-F18)	F122	Average area of triangles	This is the average area of the triangles formed by using Delaunay triangulation on the cells detected.
	F123	Std deviation of area of the triangles	This is the standard deviation of the area of the triangles formed by using Delaunay triangulation on the cells detected.

Table 5.1. Feature table,(a) texture, (b) color, (c) triangle, (d) WDD, (e) nuclei, (f) light area, (g) combined, (h, i, j, k, l) layer-by-layer triangle (Cont.)

(l) Triangle Features (Vertices as centroids but with original methods of feature F15-F18)	F124	Average edge length	This is the mean of the length of the edges of the triangles formed.
	F125	Std deviation of edge length	Standard deviation of the length of the edges of the triangles formed.

Note that feature group (h) is the completely new feature development for triangles features, and similar groups (i), (j), (k) are all control groups to test the quality of new features. And the features from F126 to F137 are basal membrane features which are not created by myself but Koyel Banerjee, and not shown in the features table presented above.

6. CLASSIFICATION

6.1 CONTINUOUS CLASSIFICATION SCALE FOR DIFFERENT FEATURE COMBINATIONS COMPUTED FROM VERTICAL

For epithelium image-based classification based on F1-F137, several neural network-based approaches have been explored by Dr. Joe Stanley and Koyel Banerjee. In the current research problem, there are four related grades for diagnostic assessment (Normal, CIN1-slightly abnormal, CIN2-moderately abnormal, CIN3-cancerous). The four grades, class labels, form a continuous range to assess the epithelium region. The research group has examined an approach to perform leave-one-out image-based classification and generate the classifier output for the left out image as a confidence value or quantitative cancer assessment, rank the confidence values for all images to provide a continuum for determining the four grades for diagnostic assessment. Scoring the image-based classifications uses the expert labeled grade for each image with the classifier generated confidence output. The classifier outputs for all images are sorted in ascending order (lower confidence corresponds to a normal epithelium and higher confidence corresponds to a cancerous epithelium). The image class labels are sorted such that normal images have the lowest confidence values, CIN1 has the next lowest range, CIN2 has the next lowest range, and CIN3 has the highest range. Based on the distribution of the confidence values, images with class labels that do not sort into the order of the confidence value range associated with each class label are called incorrect image classifications, where those images are assigned with the class label corresponding to the label associated with sorted confidence values obtained for the entire data set. This classification approach utilizes a single confidence value for each image. *Note that*

this approach is explicitly performed for exact class classification. Our research has focused on feature analysis of 10 and 5 vertical segments per image with classifier training using a leave-one-image out approach (for example, 10 vertical segments for the left out image used as the test image and the remaining 10 vertical segments per image used as the training images).

For investigating this single confidence value per image-based approach, Dr. Stanley and Koyel have investigated a Particle Swarm Optimization neural network methodology. For clarity in the experiments performed a detailed presentation of the classification algorithms is given as follows. The neural networks were trained using a leave-one-image out approach (10 vertical segments per image for 61 images gives 610 training feature vectors with individual vertical segment label assignments) and 10 vertical segments for the left out image. In order to generate a continuum of values to represent the classes normal, CIN1, CIN2, CIN3, the target outputs for each vertical segment were assigned as 0, 0.33, 0.66, 1, respectively. For each of the vertical segments (10 as an example) for the left out image, neural network outputs are determined. For combining the neural network outputs for the vertical segments for each image, the following approaches were investigated:

1) Weighted sum of the neural network outputs for the 10 vertical segments for each image
2) Hierarchical neural networks using the 10 vertical segment neural network outputs as inputs to a second tier neural network.

The weighted sum approach for combining neural network outputs is given as followed for the 10 vertical segment decomposition of each image, denoted as Seg 1, Seg

2, … , Seg 10. Let N1, N2,…, N10 denote the neural network outputs for each of the vertical segments. Let W1, W2, W3, W4, and W5 denote the weights applied to the different vertical segments. Note that the weights are specified such that the segments at corresponding positions along the medial axis are given equal weights in order to accommodate for rotational variations (flipped or not flipped) in the way that the epithelium region is processed. The final output used for each image for the 10 vertical segment case for image-based classification is given as the equation and Table 6.1 below:

$$O_{img}^{10} = \sum_{i=1}^{5} W_i N_i + W_i N_{11-i}$$

Table 6.1. Input variables for each single segment among 10 vertical segments.

Seg 1	Seg 2	Seg 3	Seg 4	Seg 5	Seg 6	Seg 7	Seg 8	Seg 9	Seg 10
N1	N2	N3	N4	N5	N6	N7	N8	N9	N10
w1	W2	W3	W4	W5	W5	W4	W3	W2	W1

The values of O_{img}^{10} are sorted for continuum based classification. Each of the weights can take on the values 0, 0.25, 0.5, 0.75, 1. "O_{img}^{10}" is calculated for different weight combinations and the continuum-based classification results are generated for each combination. Exhaustive search of the different weights combinations is performed for determining the highest classification rate. Note that different weight combinations lead to the same classification rate (linear scaling).

The same process is being investigated for 5 vertical segments decomposition for each image. Let Seg.1, Seg.2, Seg.3, Seg.4, and Seg.5 denote the 5 vertical segments. Let NN1, NN2, NN3, NN4, and NN5 denote the neural network outputs for the 5 vertical

segments, respectively, which are shown in Table 6.2. Finally, let W1, W2, and W3 denote the weights applied to the different vertical segments, again specifying the weights so that segments at corresponding positions along the medial axis are given equal weights in order to accommodate for rotational variations (flipped or not flipped) in the way that the epithelium region is processed.

Table 6.2. Input variables for each single segment among 5 vertical segments.

Seg 1	Seg 2	Seg 3	Seg 4	Seg 5
N1	N2	N3	N4	N5
w1	W2	W3	W4	W5

The final output used for each image for the 5 vertical segment case for image-based classification is given as:

$$O_{img}^{5} = W_1 N_1 + W_2 N_2 + W_3 N_3 + W_2 N_4 + W_1 N_5$$

6.2 EXPERIMENTS PERFORMED AND EXPERIMENTAL RESULTS

In this research, several experiments which reflect the classification results are performed such as leave-one out, normal vs. CIN, normal+ CIN I vs. CIN II+ CIN III, and off by one.

Leave-one out is mainly applied in training and testing which use 61 out of 62 groups of feature values to train the system in classification and take advantage of the rest one group to test whether the system gives proper classification; the training groups and testing group are different in each iteration after which the whole training and testing procedure is completed.

And normal vs. CIN, normal+ CIN I vs. CIN II+ CIN III, off by one experiments are reflected in the final results. Normal vs. CIN compare the classification result of normal and not normal (including CIN I, CIN II, CIN III stages), the results of normal+ CIN I vs. CIN II+ CIN III shows the image group which is diagnosed as normal and CIN I stage comparing with the groups which are diagnosed as CIN II and CIN III stage. Moreover, off-by-one shows the percentage of classification results which are improperly diagnosed as other stage and more than one stage off from the right stage. For example, a normal stage epithelium is diagnosed as CIN II or CIN III, vice versa.

The PSO neural network architecture with the weighted sum neural network output combination approach described above for the 10 and 5 vertical segment cases was examined for different feature combinations. Table 6.3 presents the exact class labels, the features used from Table 5.1 are listed in column 1 and 4 of Table 6.3 which give the different approaches for combining the neural network outputs for each of the vertical segments (10 vertical segments examined here).

Table 6.3. Image-based classification results using PSO neural network approach for continuous classification scale. (Note that 10 vertical segments are used for feature analysis for each image).

Features Used	Exact Class Label	Normal vs. CIN	Features Used	Exact Class Label	Normal vs. CIN
Texture	69.35	83.87	Color, Nuclei, Light Area, Combined	72.58	93.55
Correlation WDD	66.13	93.55	Color, Layer-by-Layer Triangle	53.23	77.42
Nuclei, Light Area, Combined	74.19	93.55	Color, New Triangle 2, New Triangle 3	61.29	83.87
Layer-by-Layer Triangle	48.39	74.19	Color, Basal Membrane	61.29	83.87

Table 6.3. Image-based classification results using PSO neural network approach for continuous classification scale. (Note that 10 vertical segments are used for feature analysis for each image). (Cont.)

New Triangle2	46.77	70.97	Nuclei, Light Area, Combined, Layer-by-Layer Triangle	69.35	90.32
New Triangle3	59.68	83.87	Texture, Color, Nuclei, Light Area, Combined	77.42	93.55
Basal Membrane	53.22	70.97	Texture, Color, Layer-by-Layer Triangle	77.42	96.77
Texture, Color	80.65	93.55	Texture, Color, Layer-by-Layer Triangle, Basal Membrane	74.19	93.55
Texture, Triangle	67.74	83.87	Color, Nuclei, Light Area, Combined	75.81	93.55
Texture, Correlation WDD	80.65	93.55	Correlation WDD, Nuclei, Light Area, Combined	67.74	90.32
Texture, Nuclei, Light Area, Combined	74.19	87.1	Texture, Color, Nuclei, Light Area, Combined	80.64	93.55
Texture, Layer-by-Layer Triangle	66.13	87.1	Texture, Color, Nuclei, Light Area, Combined, Combined WDD	79.03	93.55
Texture, New Triangle 2	64.52	83.87	Nuclei, Light Area, Combined, Layer-by-Layer Triangle, New Triangle 2, New Triangle 3, Basal Membrane	79.03	93.55
Texture, New Triangle 3	66.13	87.1	Texture, Color, Triangle, Nuclei, Light Area, Combined, Layer-by-Layer Triangle, Basal Membrane	83.87	96.77
Texture, Basal Membrane	66.13	87.1	Texture, Color, Triangle, Nuclei, Light Area, Combined, Combined Layer-by-Layer, New Triangle 2, Basal Membrane	88.71	96.77
Color, Correlation WDD	59.68	90.32	Texture, Color, Nuclei, Light Area, Combined, Layer-by Layer Triangle, New Triangle 3, Basal Membrane	82.26	96.77

Finally, feature analysis based on Fisher's scoring optimization technique for stepwise variable selection in SAS was performed to determine statistically significant features. Probability values (Pr) is used with the Chi-Square scores for variable selection. Note that a binary model was examined here (Normal vs. CIN) for feature selection and statistical classification of the individual vertical segments.

Based on feature reduction and examining different feature groups using 5 vertical segments for each epithelium region, the following feature combinations with classification results are presented in Table 6.4. Note that the experimental results are presented for Exact Class Label, Off-by-One Window, Normal versus CIN, and Normal versus CIN1 versus CIN2/CIN3 (3 total classes).

Table 6.4. Classification results for 5segments with different feature combinations using Exact Class Label, Off-by-One Window, Normal vs. CIN, and Normal vs. CIN1 vs. CIN2 or CIN3.

Feature Combination	Exact Class Label	Off By One Classification	Normal vs. CIN Classification	Normal vs CIN1 vs CIN2/CIN3	Segment Weights for Weighted Classifier Sum (W1,…,W5)
F1-F18, F67-F77, F124	90.32%	98.39%	96.77%	96.77%	1,0,0,0.75,0
F1-F18,F29,F30, F67-F77,F124, F126,F136	90.32%	98.39%	96.77%	96.77%	0.25,0.75,0.25,0.5,0.25

Extending the feature reduction and analysis from the 5 vertical segments, classification results for different feature groups based on 10 vertical segments are presented in Table 6.5. Again, note that the experimental results are presented for Exact

Class Label, Off-by-One Window, Normal versus CIN, and Normal versus CIN1 versus CIN2/CIN3 (3 total classes). Many different feature combinations were examined. The feature combinations presented in Table 6.5 provided the highest classification results.

Table 6.5. Classification results for different feature combinations based on 10 vertical segments using Exact Class Label, Off-by-One Window, Normal vs. CIN, and Normal vs. CIN1 vs. CIN2/CIN3.

Feature Combination	Exact Class Label	Off By One Classification	Normal vs. CIN Classification	Normal vs CIN1 vs CIN2/CIN3	Segment Weights for Weighted Classifier Sum (W1,…,W5)
F1-F18, F67-F77	91.94%	100.00%	96.77%	96.77%	1,0,0,0.75,0
F1-F18, F67-F77,F124,F126,F136	88.71%	100.00%	96.77%	93.55%	1,0.5,0,1,1
F1-F18,F29,F30,F67-F77, F124,F126,F136	85.48%	100.00%	96.77%	90.32%	0.25,0,0.75, 0,0.25

Table 6.4 and Table 6.5 show actual image classification rates of 90.32% and 91.94% for the 5 and 10 vertical segment cases, respectively. The feature combinations that yielded the highest classification results for the 10 and 5 vertical segment cases include the texture features (F1-F11), color features (F12-F14), triangle features (F15-F18), nuclei features (F67,F68), light area features (F69-F75), and combined features (F76,F77).

6.3 INTER-PATHOLOGIST IMAGE-BASED CLASSIFICATION OF DIGITIZED CERVICAL IMAGE DATA SET

Dr. Rosemary Zuna, Professor of Pathology, at the University of Oklahoma Health Sciences Center provided the expert pathologist CIN grades for the 62 digitized histology images of the epithelium region presented in the previous sections of this thesis.

In this section and in following sections, a second expert pathologist was sought for guidance in establishing CIN truth classifications for sub-regions of the epithelium (individual vertical segments) and for the entire epithelium region. Dr. Shelly Frazier, Surgical Pathologist, at the University of Missouri was approached and agreed to provide these classifications for the 62 cervical images data set. Note that all vertical segment classifications used in this study were provided by Dr. Shelly Frazier, Dr. Zuna and Dr. Frazier provided whole image CIN grades.

Overall, the CIN classification results from Table 6.5 before and Table 6.6 below are similar, with slightly higher classification results obtained based on the expert CIN labeling from Dr. Zuna. Using Dr. Frazier's CIN labeling of the 62 image data set with 10 and 5 vertical segments, several features set combinations were examined using different scoring schemes, including the Exact Class Label, Normal vs. CIN and Normal+CIN1 vs. CIN2+CIN3.

Table 6.6. Classification results based on CIN truth grades from Dr. Frazier for different feature combinations based on 10 vertical segments using Exact Class Label, Off-by-One Window, Normal vs. CIN, and Normal vs. CIN1 vs. CIN2/CIN3.

Feature Combination	Actual Image Classification	Off By One Classification	Normal vs. CIN Classification	Normal vs CIN1 vs CIN2/CIN3	Segment Weights for Weighted Classifier Sum (W1,…,W5)
F1-F18, F67-F77	88.71%	98.39%	96.77%	91.94%	1,0.25,1,0.25,0
F1-F18, F67-F77, F124,F126,F136	88.71%	98.39%	96.77%	93.55%	1,0.5,0,1,1

The individual 5 vertical segment CIN labels for classifier training were the image-based CIN labels provided by Dr. Frazier. Koyel and I used the same PSO-based classifier to train and test the images with leave one image out scheme.

The following parameters were used in the PSO neural network algorithm:

rg_vals = 0.001, rm_vals = 0.001, c2_vals = 1.5;

c1_vals = 1, particles_number_vals = 30, w_vals = 0.6;

Tables 6.7 and 6.8 present the classification results for the different features.

Table 6.7. Classification results for different feature combinations with 10 vertical segments for Exact Class Label, Normal vs. CIN, and CIN1 vs. CIN2/CIN3 based on Dr. Frazier's CIN labeling.

Features Used	Exact Class Label	Normal vs. CIN	Normal + CIN I vs. CIN II + CIN III	Features Used	Exact Class Label	Normal vs. CIN	Normal + CIN I vs. CIN II + CIN III
Texture	69.35	83.87	83.87	Nuclei, Light Area, Combined, Layer-by-Layer Triangle	69.35	90.32	91.94
Texture, Color, Triangle, Nuclei, Light Area, Combined, Layer-by-Layer Triangle, Basal Membrane	88.71	96.77	93.55	Texture, Triangle	67.74	83.87	83.87
Texture, Color, Nuclei, Light , Combined, Layer-by Layer Triangle, Basal Membrane	82.26	96.77	93.55	Correlation WDD, Nuclei, Light Area, Combined	67.74	90.32	91.94

Table 6.7. Classification results for different feature combinations with 10 vertical segments for Exact Class Label, Normal vs. CIN, and CIN1 vs. CIN2/CIN3 based on Dr. Frazier's CIN labeling. (Cont.)

Texture, Color	80.65	93.55	91.94	Correlation WDD	66.13	93.55	93.55
Texture, Correlation WDD	80.65	93.55	93.55	Texture, New Triangle 3	66.13	87.1	83.87
Texture, Color, Nuclei, Light Area, Combined	80.64	93.55	95.16	Texture, Basal Membrane	66.13	87.1	82.26
Texture, Color, Nuclei, Light Area, Combined, Combined WDD	79.03	93.55	91.94	Texture, New Triangle 2	66.13	87.1	85.48
Nuclei, Light Area, Combined, Layer-by-Layer Triangle, New Triangle 2, New Triangle 3, Basal Membrane	79.03	93.55	91.94	Color, New Triangle 2, New Triangle 3	61.29	83.87	82.26
Color, Nuclei, Light Area, Combined	72.58	93.55	87.1	New Triangle2	46.77	70.97	72.58

From Table 6.7, the best 10 vertical segment classification results are 88.71% for the Exact Class Label, 95.16% for CIN vs. Normal and 93.55% for Normal+CIN I vs. CIN II + CIN III. From Table 6.8, the best 5 vertical segment classification results are 90.32% for the Exact Class Label, 96.77% for CIN vs. Normal and 96.77% for Normal + CIN I vs. CIN II + CIN III.

Table 6.8. Classification results for different feature combinations with 5 vertical segments for Exact Class Label, Normal vs. CIN, and CIN1 vs. CIN2/CIN3 based on Dr. Frazier's CIN labeling.

Features Used	Exact Class Label	Normal vs. CIN	Normal + CIN I vs. CIN II + CIN III	Features Used	Exact Class Label	Normal vs. CIN	Normal + CIN I vs. CIN II + CIN III
Texture, Color, Nuclei, Light Area, Combined, Layer-by Layer Triangle, New Triangle 3, Basal Membrane	90.32	96.77	96.77	Texture, Color, Layer-by-Layer Triangle	83.87	93.55	91.94
Texture, Color, Nuclei, Light Area, Combined	88.71	96.77	96.77	Texture, Color, Nuclei, Light Area, Combined, Combined WDD	83.87	93.55	95.16
Texture, Color, Triangle, Nuclei, Light Area, Combined, Layer-by-Layer Triangle, Basal Membrane	88.71	96.77	96.77	Nuclei, Light Area, Combined, Layer-by-Layer Triangle, New Triangle 2, New Triangle 3, Basal Membrane	77.42	96.77	93.55
Texture, Color	87.1	93.55	96.77	Texture, Correlation WDD	74.19	90.32	87.1
Texture, Triangle	83.87	83.87	90.16				

The combination of features which yielded the highest classification results contains texture, color, nuclei, light area, combined features, triangle, and only three features in the group of basal membrane features. Texture and color feature provide the general situation with respect to the whole epithelium including color data and structural analysis data. Nuclei, light area, and combined features, as well as triangle features give much information about the characters in different CIN stages, they are more dynamic and differ with the increasing of CIN stage with which a clue can be found in contributing to make a proper diagnosis.

The other group of features like Correlation WDD, Triangle features discussed in former paper, and most of the basal membrane do not yield as good a result as those mentioned above do. And, the basal membrane feature is a little different from other features but also follow the rules that features are operated in different layers, which finally give information about the origin of certain CIN stages. With some concern, these features fail to provide some “key information” which leads a significant difference in describing the current situation of the whole epithelium, or in other words, are not typical or universal for all the epithelium regions which are taken into the test. Some of the features are generated to be trials or control group, in order to discover more clues which can lead to a better result.

According to the results which are presented in the former paper, feature combination of texture, original triangle and correlation WDD features yielded the exact label classification result of 70.5% and normal vs. CIN result to be 90.2%. As a matter of fact, the recent research does yield much better results with exact label classification result of 90.32% and normal vs. CIN to be 96.77% compared with previous results.

7. ANALYSIS OF INTER-PATHOLOGIST EPITHELIUM CLASSIFICATION

In this section, all the research and analysis are completed by myself, by using detail comparison and analysis to present the situation of the classification results that are given by the pathologists, in order to get more related information about the contribution of the single segments to the final classification results and the relationship between classification results and the whole algorithm. These CIN truth references are examined for comparison with the reference truth reference in evaluating the features developed. From Table 7.1, there are 5 images (in bold) where the expert (Dr. Zuna) and Dr. Frazier differed in CIN truth. In all 5 cases, the expert labeled CIN grade differed by 1 CIN grade value. In examining the CIN truth references, there are 10 segments for each of the 62 images, so there are 620 classifications of single segments (individual vertical segments) to be discussed and described. I divide the individual vertical segments into several categories to make it much clearer and easier. All the categories are presented below:

- The classification results in both experts agree with each other on whole image classification (7.1)
  - Non-zero (all segments within an image have valid CIN grade classifications) existing in any one of the 10 segments for one whole image (7.1.1)
    - One same CIN grade for all 10 segments of one whole image
    - Multi-CIN grades among 10 segments for an image
      - 10 segments result distributed in 2 different levels
      - 10 segments result distributed in 3 different levels
  - Zero existing in any one of the 10 segments (7.1.2)

- Only one zero existing among 10 segments result of one whole image
- More than one zeros existing among 10 segments result of one whole image

- The classification results in which two experts disagree with each other(7.2)

All the classification results will be shown in the form of tables with Cervical Intraepithelial Neoplasia grading scales marked as "1 = Normal, 2 = CIN 1, 3 = CIN 2, 4 = CIN 3, 0 = inconclusive CIN grade assignment", also the image name is given as well as every single segment from it. All the different categories given above are marked with different group titles which are shown in the end of every category description.

7.1. THE CLASSIFICATION RESULTS IN BOTH EXPERTS AGREE WITH EACH OTHER ON WHOLE IMAGE CLASSIFICATION

7.1.1. Non-zero Existing in Any One of the 10 Segments. There is a same CIN grade for all the 10 segments of one whole image, for each of the 23 images in this group, the image-based classification is given from both of the experts (NLM Expert Classification from Dr. Rosemary Zuna from the University of Oklahoma Health Sciences Center and Dr. Shelly Frazier from the University of Missouri) and 10 single vertical segment classifications are given by Dr. Frazier. Also, all the 10 segment results stay the same and agree with the final classification grading scale for the whole image. All the images in this group are presented below ranked in order of CIN grading scale from "1" to "4".

In Table 7.1, there are 11 images where the two experts agree with each other again on the classification assignment. All the classification assignments for the single segments are “1” (Normal), for the reason that the nuclei distribution is relatively clear, not a significant number of nuclei, and the nuclei are highly concentrated on the basal membrane part of the epithelium. In addition, for these images, there is considerable area of light region (white area) and it remains solid red for the surface color.

Table 7.1. Both experts agree on whole image and individual segment normal grade classification (11 images total).

Image Name	NLM Expert Classifications	Dr. Shelly Frazier Classifications		Cervical Intraepithelial Neoplasia grading scale 1 = Normal 2 = CIN 1 3 = CIN 2 4 = CIN 3	
ouhsc_d15-3-normal	**1**	**1**			
					10 segments of one whole image, and the individual manual classification label from Dr. Frazier
1	1	1	1	1	
1	1	1	1	1	

Table 7.1. Both experts agree on whole image and individual segment normal grade classification (11 images total). (Cont.)

ouhsc_d3-4-normal	**1**	**1**		
			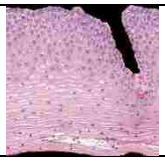	
1	1	1	1	1
ouhsc_d4-1-normal	**1**	**1**		
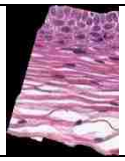	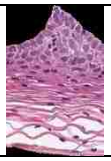	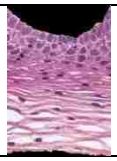	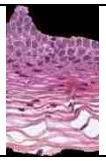	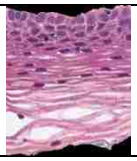
1	1	1	1	1
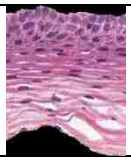		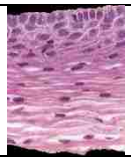		
1	1	1	1	1
ouhsc_d55-4-normal	**1**	**1**		
	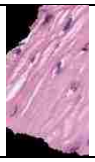	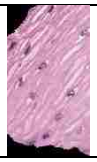		
1	1	1	1	1
1	1	1	1	1

Table 7.1. Both experts agree on whole image and individual segment normal grade classification (11 images total). (Cont.)

Image Name	NLM Expert Classifications	Dr. Shelly Frazier Classifications		Cervical Intraepithelial Neoplasia grading scale 1 = Normal 2 = CIN 1 3 = CIN 2 4 = CIN 3	
ouhsc_d61-2-normal	1	1			
					10 segments of one whole image, and the individual manual classification label from Dr. Frazier
1	1	1	1	1	
1	1	1	1	1	
ouhsc_d61-3-normal	1	1			
		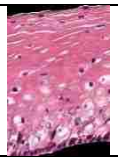	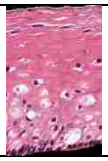	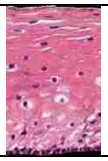	
1	1	1	1	1	
	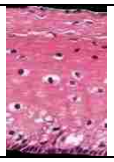	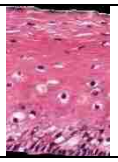	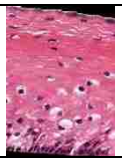		
1	1	1	1	1	
ouhsc_d61-4-normal	1	1			
1	1	1	1	1	
1	1	1	1	1	

Table 7.1. Both experts agree on whole image and individual segment normal grade classification (11 images total). (Cont.)

ouhsc_d8-1 -normal	1	1		
1	1	1	1	1
1	1	1	1	1

ouhsc_d8-3 -normal	1	1		
1	1	1	1	1
1	1	1	1	1

ouhsc_d8-4 -normal	1	1		
1	1	1	1	
1	1	1	1	1

Table 7.1. Both experts agree on whole image and individual segment normal grade classification (11 images total). (Cont.)

ouhsc_d65-2-normal	1	1		
1	1	1	1	1
1	1	1	1	1

In Table 7.2, there are 5 images that both experts classified as CIN1. For these images, all 10 segments for each image are labeled as CIN 1 by the experts (Dr. Frazier's individual segment classifications are shown in Table 3). For these images, the light area becomes less (compared to normal grade images) and the nuclei start to grow across the epithelium. In addition, the color of the region of interest tends to be darker (than normal images).

In Table 7.3 later after Table 7.2, there are 4 images in the 62 image data set where both experts agree on CIN 2 grades for the whole image and CIN 2 for all of the individual segments within those images. Some observations about these images that have agreed CIN 2 grades from both experts include these: 1) a dark nuclei are intensively concentrated in the basal membrane part and spread out through the middle part towards the whole epithelium, 2) darker color with even less light area surround the nuclei, and the nuclei closer to the bottom are relatively sparse all of which contributes to CIN 2 classification.

Table 7.2. Experts both agree on CIN 1 grades for whole image and all segments have CIN 2 grades (5 images total).

Image Name	NLM Expert Classifications	Dr. Shelly Frazier Classifications		Cervical Intraepithelial Neoplasia grading scale 1 = Normal 2 = CIN 1 3 = CIN 2 4 = CIN 3	
ouhsc_d55-3-cin1	2	2			
					10 segments of one whole image, and the individual manual classification label from Dr. Frazier
2	2	2	2	2	
2	2	2	2	2	

Image Name	NLM Expert Classifications	Dr. Shelly Frazier Classifications		Cervical Intraepithelial Neoplasia grading scale 1 = Normal 2 = CIN 1 3 = CIN 2 4 = CIN 3	
ouhsc_d74-2-cin1	2	2			
					10 segments of one whole image, and the individual manual classification label from Dr. Frazier
2	2	2	2	2	
2	2	2	2	2	

Table 7.2. Experts both agree on CIN 1 grades for whole image and all segments have CIN 2 grades (5 images total). (Cont.)

ouhsc_lsil3-1-cin1	2	2		
2	2	2	2	2
2	2	2	2	2

ouhsc_lsil4-1-cin1	2	2		
2	2	2	2	2
2	2	2	2	2

ouhsc_d65-6-cin1	2	2		
2	2	2	2	2
2	2	2	2	2

Table 7.3. Experts both agree on CIN 2 labels on whole image and individual segment grades (4 images total).

Image Name	NLM Expert Classifications	Dr. Shelly Frazier Classifications		Cervical Intraepithelial Neoplasia grading scale 1 = Normal 2 = CIN 1 3 = CIN 2 4 = CIN 3	
ouhsc_d14-2-cin2	3	3			
					10 segments of one whole image, and the individual manual classification label from Dr. Frazier
3	3	3	3	3	
3	3	3	3	3	

Image Name	NLM Expert Classifications	Dr. Shelly Frazier Classifications		Cervical Intraepithelial Neoplasia grading scale 1 = Normal 2 = CIN 1 3 = CIN 2 4 = CIN 3	
ouhsc_d4-2-cin2	3	3			
			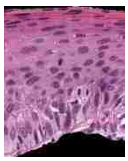	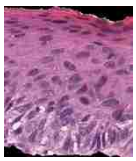	10 segments of one whole image, and the individual manual classification label from Dr. Frazier
3	3	3	3	3	
	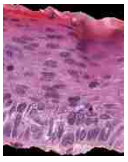				
3	3	3	3	3	

Table 7.3. Experts both agree on CIN 2 labels on whole image and individual segment grades (4 images total). (Cont.)

Image Name	NLM Expert Classifications	Dr. Shelly Frazier Classifications		Cervical Intraepithelial Neoplasia grading scale 1 = Normal 2 = CIN 1 3 = CIN 2 4 = CIN 3	
ouhsc_d4-3-cin2	3	3			
					10 segments of one whole image, and the individual manual classification label from Dr. Frazier
3	3	3	3	3	
3	3	3	3	3	

Image Name	NLM Expert Classifications	Dr. Shelly Frazier Classifications		Cervical Intraepithelial Neoplasia grading scale 1 = Normal 2 = CIN 1 3 = CIN 2 4 = CIN 3	
ouhsc_d65-4-cin2	3	3			
					10 segments of one whole image, and the individual manual classification label from Dr. Frazier
3	3	3	3	3	
		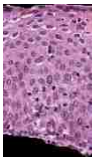			
3	3	3	3	3	

From Table 7.4 below, there are 3 images that both experts provided CIN 3 grades, with all 10 segments from each image labeled as CIN 3. Common characteristics of these images include: light areas are uncommon, nuclei intensively growing across the epithelium from top to bottom, and the solid reddish color becomes more blackish.

Table 7.4. Experts both agree on CIN 3 labels on whole image and individual segment grades (3 images total).

Image Name	NLM Expert Classifications	Dr. Shelly Frazier Classifications		Cervical Intraepithelial Neoplasia grading scale 1 = Normal 2 = CIN 1 3 = CIN 2 4 = CIN 3	
ouhsc_d61-1-cin3	4	4			
					10 segments of one whole image, and the individual manual classification label from Dr. Frazier
4	4	4	4	4	
4	4	4	4	4	
ouhsc_d68-2-cin3	4	4			
4	4	4	4	4	
4	4	4	4	4	

Table 7.4. Experts both agree on CIN 3 labels on whole image and individual segment grades (3 images total). (Cont.)

Image Name	NLM Expert Classifications	Dr. Shelly Frazier Classifications		Cervical Intraepithelial Neoplasia grading scale 1 = Normal 2 = CIN 1 3 = CIN 2 4 = CIN 3	
ouhsc_cin1-1-1-cin1	4	4			
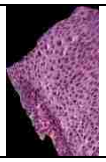	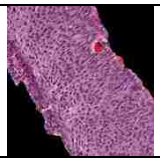	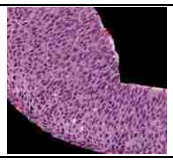	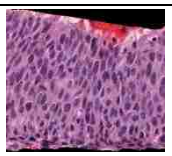	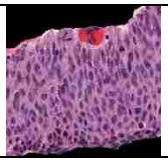	10 segments of one whole image, and the individual manual classification label from Dr. Frazier
4	4	4	4	4	
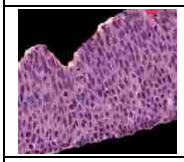	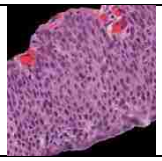	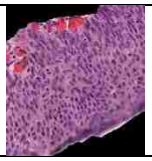	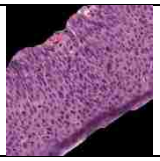	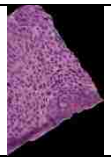	
4	4	4	4	4	

◆ Segments result distributed in 2 different levels

In this category of image classifications, both experts agree on the whole image CIN label, but the individual segments have different CIN grades (some segment assignments agree with the whole image CIN label). For each of the 15 images, the CIN classifications for both experts agree for the whole image, but the CIN classifications for the different segments are not all the same as the whole image classification. Table 7.5 below presents CIN labels for Dr. Zuna (NLM Expert) and Dr. Frazier for the whole image and the individual segment CIN grades determined by Dr. Frazier for 15 images.

Table 7.5. Whole image and individual segment CIN classifications for 15 images where both experts agree on the whole image classification and the individual segment classifications vary from the whole image.

Image Name	NLM Expert Classifications	Dr. Shelly Frazier Classifications		Cervical Intraepithelial Neoplasia grading scale 1 = Normal 2 = CIN 1 3 = CIN 2 4 = CIN 3	
ouhsc_d26-1-cin3	4	4			
		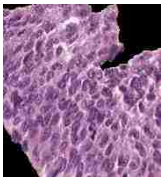			10 segments of one whole image, and the individual manual classification label from Dr. Frazier
3	3	3	3	3	
	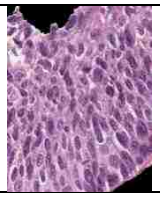				
3	3	3	4	4	

Image Name	NLM Expert Classifications	Dr. Shelly Frazier Classifications		Cervical Intraepithelial Neoplasia grading scale 1 = Normal 2 = CIN 1 3 = CIN 2 4 = CIN 3	
ouhsc_d26-2-cin3	4	4			
					10 segments of one whole image, and the individual manual classification label from Dr. Frazier
3	3	4	4	3	
4	3	3	4	3	

Table 7.5. Whole image and individual segment CIN classifications for 15 images where both experts agree on the whole image classification and the individual segment classifications vary from the whole image. (Cont.)

ouhsc_d4-4-cin2	3	3		
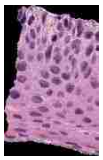	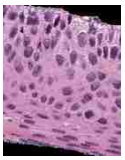		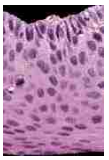	
3	3	3	3	3
3	3	4	3	3
ouhsc_d49-1-cin2	3	3		
		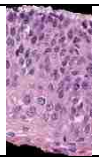		
3	3	3	3	3
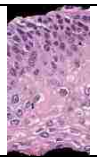			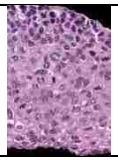	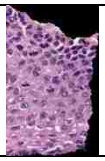
3	2	3	3	3
ouhsc_d49-2-cin1	2	2		
2	2	1	2	2
2	2	1	2	1

Table 7.5. Whole image and individual segment CIN classifications for 15 images where both experts agree on the whole image classification and the individual segment classifications vary from the whole image. (Cont.)

ouhsc_d56-1-cin3	4	4		
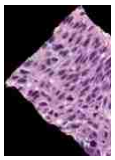	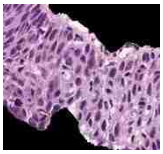	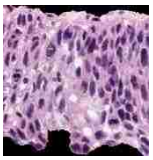		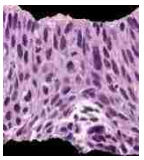
4	4	3	4	4
	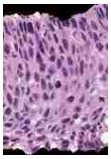	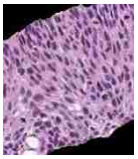	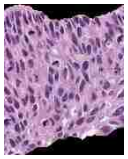	
4	3	4	4	4
ouhsc_d62-1-cin1	2	2		
1	1	2	2	2
2	2	1	2	2
ouhsc_d62-4-cin3	4	4		
3	4	4	4	4
4	4	4	3	4

Table 7.5. Whole image and individual segment CIN classifications for 15 images where both experts agree on the whole image classification and the individual segment classifications vary from the whole image. (Cont.)

ouhsc_d68-1-cin3	4	4		
4	4	4	4	4
4	4	4	4	3
ouhsc_d68-4-cin3	4	4		
4	4	3	4	4
4	3	3	4	4
ouhsc_d74-1-cin3	4	4		
4	4	4	4	4
3	4	4	4	3

Table 7.5. Whole image and individual segment CIN classifications for 15 images where both experts agree on the whole image classification and the individual segment classifications vary from the whole image. (Cont.)

ouhsc_d84-1-cin3	4	4		
4	3	3	3	3
3	3	3	3	3
ouhsc_lsil3-2-cin1	2	2		
2	2	2	2	2
2	2	1	1	1
ouhsc_d84-2-cin3	4	4		
4	4	4	4	4
4	4	3	4	4

Table 7.5. Whole image and individual segment CIN classifications for 15 images where both experts agree on the whole image classification and the individual segment classifications vary from the whole image. (Cont.)

ouhsc_d15-2-cin2	3	3			
	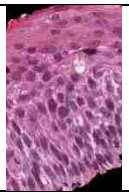	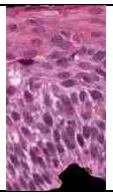			10 segments of one whole image, and the individual manual classification label from Dr. Frazier
2	2	2	2	2	
2	2	3	3	3	

The goal of analysis in this subsection is to address characteristics of the whole image CIN classification that can be extracted from the individual segment CIN classifications, particularly when the individual segment CIN classifications vary.

For example in Table 7.5, in the image ("ouhsc_d15-2-cin2"), most of the individual segments are labeled as "2" (CIN 1) by the expert pathologists, but the whole image is labeled as "3" (CIN 2). Thus, the final CIN label is not necessarily determined by the classifications of the individual segments, but by the composite of individual segment information. In order words, the whole image is labeled as a CIN 2 if it shows enough CIN 2 characteristic features, withstanding the number of individual segments that may locally characteristic of another CIN grade.

- 10 segments result distributed in 3 different levels

In this category of classification results which are shown in Table 7.6, the situation becomes a little more complicated where 10 segment results are distributed in 3 different CIN stages. An image result description is given below as an example:

In image “ouhsc_d15-1-cin3”, both expert classification results are “4”(CIN 3). However, it can be observed from Table 7.6 that Dr. Frazier’s individual segment classifications for the 10 are distributed in three different grading levels, the first 3 segments as “4”(CIN 3) and the others as “3” and “2” differently. According to the first three classification results which have the highest grading level of “4”(CIN 3) and contain the mid part of the whole epithelium which occupies the major useful information, impacting the whole image CIN classification.

Table 7.6. Whole image and individual segment CIN classifications for 9 images where both experts agree on the whole image classification and the individual segment classifications vary from the whole image.

Image Name	NLM Expert Classifications	Dr. Shelly Frazier Classifications		Cervical Intraepithelial Neoplasia grading scale 1 = Normal 2 = CIN 1 3 = CIN 2 4 = CIN 3	
ouhsc_d15-1-cin3	4	4			
					10 segments of one whole image, and the individual manual classification label from Dr. Frazier
4	4	4	3	2	
2	2	3	3	3	

Table 7.6. Whole image and individual segment CIN classifications for 9 images where both experts agree on the whole image classification and the individual segment classifications vary from the whole image. (Cont.)

ouhsc_d3-2-cin2	3	3		
				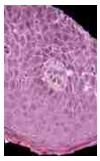
1	1	2	1	2
		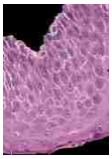		
1	2	2		
ouhsc_d3-1-cin3	4	4		
2	3	4	3	3
4	3	4	3	4
ouhsc_d55-1-cin2	3	3		
1	2	3	3	2
3	3	3	3	2

Table 7.6. Whole image and individual segment CIN classifications for 9 images where both experts agree on the whole image classification and the individual segment classifications vary from the whole image. (Cont.)

ouhsc_d55-2-cin2	3	3		
1	2	2	2	3
1	1	1	1	2
ouhsc_d62-2-cin2	3	3		
1	2	3	2	3
3	3	3	3	3
ouhsc_d62-3-cin2	3	3		
3	3	2	3	2
		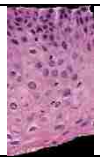		
2	2	2	2	1

Table 7.6. Whole image and individual segment CIN classifications for 9 images where both experts agree on the whole image classification and the individual segment classifications vary from the whole image. (Cont.)

ouhsc_d62-5-cin3	4	4		
2	2	3	3	4
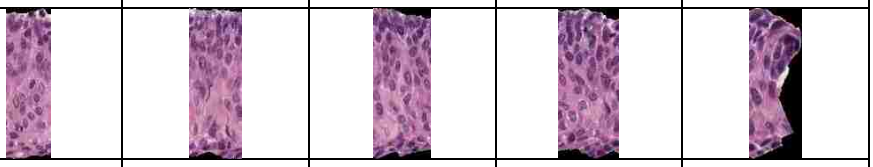				
4	3	3	4	3
ouhsc_d65-5-cin2	3	3		
1	2	2	2	2
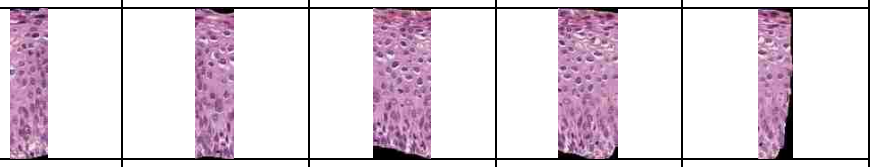				
3	3	3	3	2

7.1.2 Zero Existing in Any One of the 10 Segments. Firstly, for the situation of "only one zero existing among 10 segments result of one whole image", there are 4 images where experts agree on the CIN grades for the whole image and Dr. Frazier labeled one of the individual segments as "0", meaning that the segment was too small or did not include enough information to make a CIN grade assignment.

For the 4 images or 40 segments presented in Table 7.7, "zero-image" can be easily found where only a little part of the whole epithelium is located. Also, enough

information from a complete slice of the epithelium can't be addressed from it. Here are the zero-images shown in Figure 7.1.

0	0	0	0

Figure 7.1. Single segments which are given "0".

Compared to the other images which are given a certain CIN grade, the "zero-images" are always lack of the ability of showing enough useful information about the basal membrane, the nuclei, and the light area at the same time, by which a proper decision can be finally made.

Table 7.7. Whole image and individual segment CIN classifications for 4 images where both experts agree on the whole image classification with an inconclusive individual segment classification ("0").

Image Name	NLM Expert Classifications	Dr. Shelly Frazier Classifications		Cervical Intraepithelial Neoplasia grading scale 1 = Normal 2 = CIN 1 3 = CIN 2 4 = CIN 3	
ouhsc_d3-3-cin2	3	3			
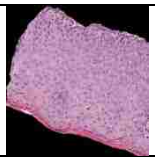		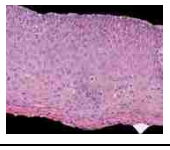	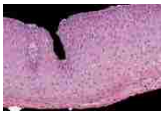	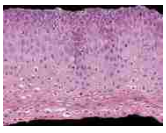	10 segments of one whole image, and the individual manual classification label from Dr. Frazier
0	3	3	3	3	
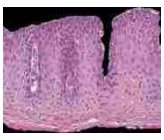	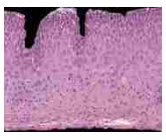	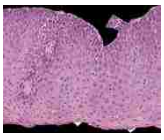	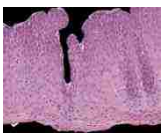		
3	3	3	3	3	

Table 7.7. Whole image and individual segment CIN classifications for 4 images where both experts agree on the whole image classification with an inconclusive individual segment classification (“0”). (Cont.)

ouhsc_cin1-1-1-cin1	2	2		
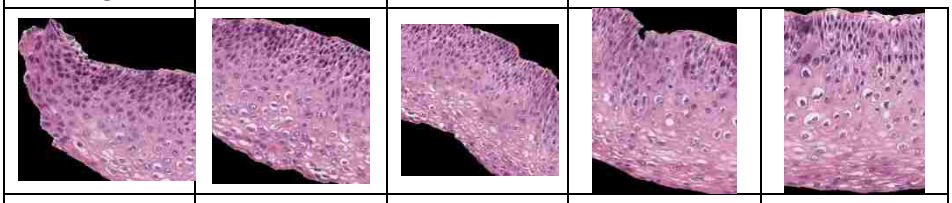				
2	2	2	2	2
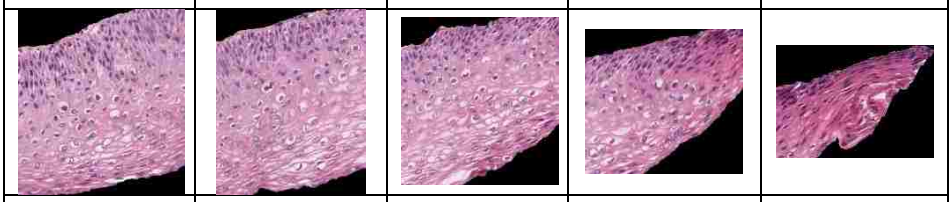				
2	2	2	2	0
ouhsc_d68-5-cin3	4	4		
4	4	4	4	3
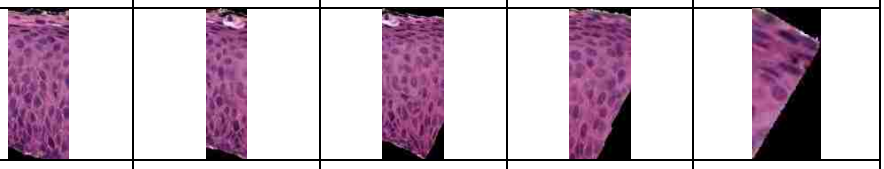				
3	4	3	4	0
ouhsc_lsil2-1-cin1	2	2		
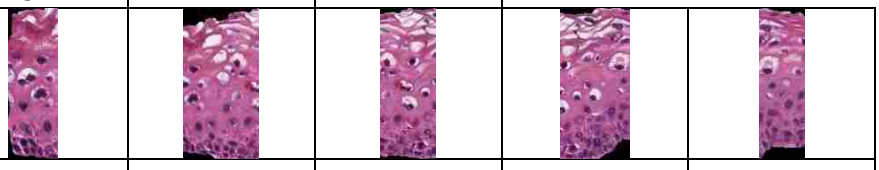				
2	2	2	2	2
2	2	2	2	0

For example from Table 7.7 before, Dr. Frazier and Dr. Zuna classify image "ouhsc_lsil2-1-cin1" as a CIN 1, where it can be observed that most of the nuclei are located at the top third part of the whole epithelium. Based on Dr. Frazier's individual segment classifications, the 10th segment (end segment) is classified as "0", as it is seen that only a little part of the epithelium is shown and maybe there is not enough information provided for a proper classification.

- More than one zeros existing among 10 segments result of one whole image

In this category of images there are multiple inconclusive individual segments ("0" classifications), which make this category are more complicated than in last group presented. Table 7.8 presents the 5 images from the 62 image data set with multiple cases of inconclusive individual segments.

Table 7.8. Whole image and individual segment CIN classifications for 4 images where both experts agree on the whole image classification with an inconclusive individual segment classification ("0").

Image Name	NLM Expert Classifications	Dr. Shelly Frazier Classifications		Cervical Intraepithelial Neoplasia grading scale 1 = Normal 2 = CIN 1 3 = CIN 2 4 = CIN 3	
ouhsc_d49-4-normal	1	1			
		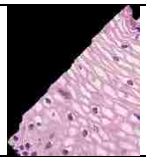	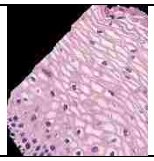	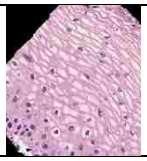	10 segments of one whole image, and the individual manual classification label from Dr. Frazier
0	0	1	1	1	
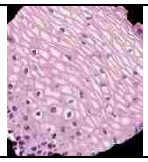	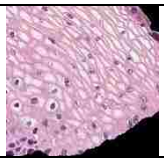	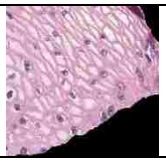	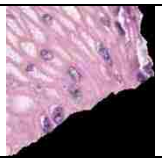		
1	1	1	1	0	

Table 7.8. Whole image and individual segment CIN classifications for 4 images where both experts agree on the whole image classification with an inconclusive individual segment classification (“0”). (Cont.)

ouhsc_d50-2-normal	1	1		
			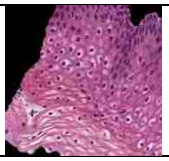	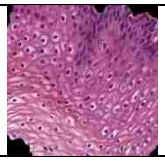
0	1	1	1	1
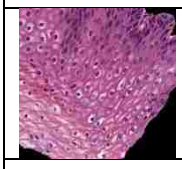	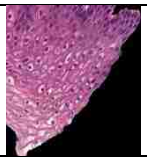	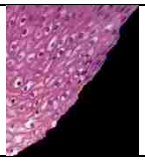		
1	1	1	0	0

ouhsc_gas-10541-2-normal	1	1		
				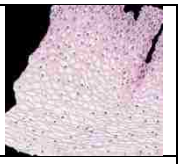
0	0	1	1	1
	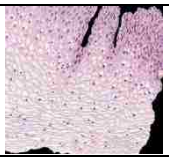			
1	1	1	1	0

ouhsc_gas-10541-1-cin1	2	2		
		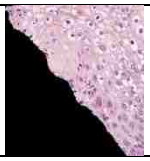	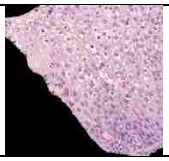	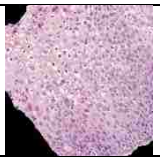
0	0	2	2	2
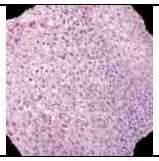	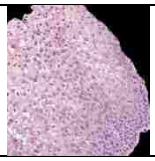		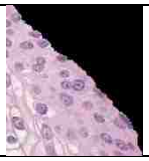	
2	2	2	2	0

Table 7.8. Whole image and individual segment CIN classifications for 4 images where both experts agree on the whole image classification with an inconclusive individual segment classification (“0”). (Cont.)

ouhsc_lsil3-3-cin1	2	2		
	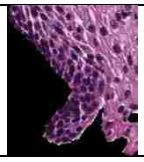	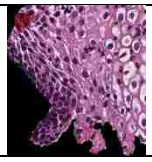	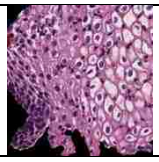	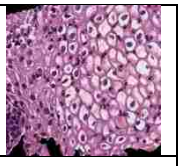
0	2	2	2	2
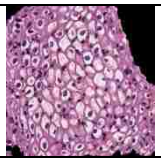	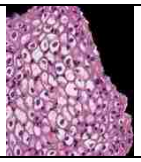	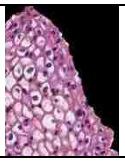		
2	2	2	0	0

From Table 7.8, the tables of individual segments seem to be not completed, ① with some blocks empty but, at the same time, with a “0” result at the bottom of them; ② some blocks are not empty still with a “0” as a result.

Here it has to be clear, that the blocks which are not empty but with a “0” result because the content or segment image of that block does not provide enough information for a proper diagnose.

The empty blocks (individual segments) are generated by the bounding box algorithm developed and presented in a previous statement of work, which divides the whole image into 10 vertical segments. During the progress of generating 10 segments, 10 bounding boxes are drawn across the medial axis to contain each part of the 10 segments. The empty bounding boxes are always located at both ends of left and right direction, which explains why the empty blocks (or bounding boxes) are always the

first(or last) one or two. The bounding box algorithm divides the medial axis into tenths for obtaining the 10 vertical segments. One of the difficulties in developing the bounding box and other techniques is that the ends of the epithelium region are often oriented differently than the interior portion of the epithelium region. When the vertical segments are extracted based on the medial axis partitioning into tenths, the area of the end vertical segments is often less than the interior vertical segments extracted. A potential approach to address this problem is to estimate the area of each vertical segment in determining where to partition the medial axis for vertical segment extraction such as partitioning the medial axis to obtain approximately equal area vertical segments. However, the number of individual segments with label "0" does not appear to impact the whole image CIN classifications, which is shown in Table 7.9. And the final CIN classification is obtained using the same approach presented in Section 7.1.2.

Table 7.9. Image example with end segments as inconclusive ("0") where both experts agree on the whole image classification.

Image Name	NLM Expert Classifications	Dr. Shelly Frazier Classifications		Cervical Intraepithelial Neoplasia grading scale 1 = Normal 2 = CIN 1 3 = CIN 2 4 = CIN 3	
ouhsc_d49-4-normal	1	1			
					10 segments of one whole image, and the individual manual classification label from Dr. Frazier
0	4	4	4	4	
4	4	4	4	0	

7.2 THE CLASSIFICATION RESULTS IN WHICH TWO EXPERTS DISAGREE WITH EACH OTHER

In this category, 3 images (given in Table 7.10) are shown in which two experts give different CIN classifications (within 1 CIN grade) for the whole image classification. For all of these images, the experts differ by 1 CIN grade, meaning that the experts have very similar diagnostic interpretations. Also, note that Dr. Frazier has a consistently more conservative classifications (1 CIN grade higher) than Dr. Zuna.

"Zero images" appear here again in this group of images, and the reason is explained in the former group that the bounding boxes have nothing inside because of the small size of images.

Table 7.10. Whole image CIN classifications on which the experts disagree with each other.

Image Name	NLM Expert Classifications	Dr. Shelly Frazier Classifications		Cervical Intraepithelial Neoplasia grading scale 1 = Normal 2 = CIN 1 3 = CIN 2 4 = CIN 3	
ouhsc_d46-2-normal	1	2			
		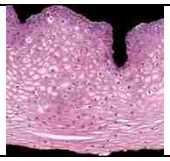		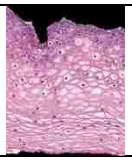	10 segments of one whole image, and the individual manual classification label from Dr. Frazier
1	1	1	1	1	
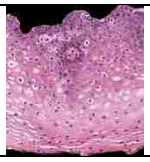	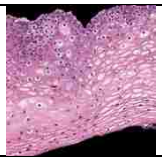	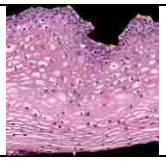	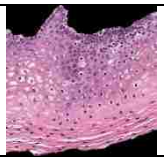		
1	1	1	1	1	

Table 7.10. Whole image CIN classifications on which the experts disagree with each other. (Cont.)

Image Name	NLM Expert Classifications	Dr. Shelly Frazier Classifications		Cervical Intraepithelial Neoplasia grading scale 1 = Normal 2 = CIN 1 3 = CIN 2 4 = CIN 3	
ouhsc_d49-3-normal	1	2			
		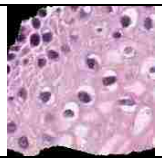			10 segments of one whole image, and the individual manual classification label from Dr. Frazier
0	1	1	1	1	
1	1	1	0	0	
ouhsc_gas-10541-3-cin1	2	3			
		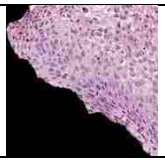	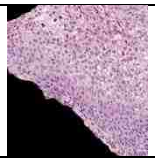	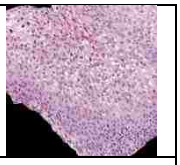	
0	0	2	2	2	
		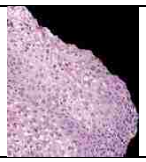	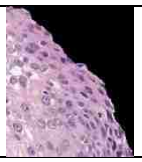		
2	2	2	2	0	

And the most interesting thing is, according to the segmentation results from two experts that they agree with each other because all the segmentation results for the whole images are the same with the final result from NLM expert. But the only thing different is the final classification result from Dr. Frazier who gives it a higher CIN grading level

than the segment results; like in image “ouhsc_d46-2-normal”, all the segment results are “1” (Normal) but the final result shows to be “2” (CIN1).

From examining all of the categories presented in this report, the individual segments can be interpreted as specific CIN grades reasonably. However, the image examples show that the individual segment classifications can vary within an image and are required to be interpreted in the context of whole image to facilitate the whole image CIN classification.

The images shown below in Figure 7.2 are the 3 images from which the 10 segments of each image are generated; they look different because they are in a condition before segmenting the epithelium out from the image. Also, these are the images from which the experts drew their final classification results.

ouhsc_d49-3-normal

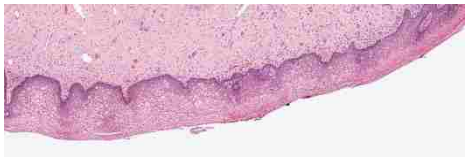

ouhsc_d46-2-normal

ouhsc_gas-10541-3-cin1

Figure 7.2. Whole image examples.

Table 7.11 presents 2 image examples where the experts differ in the whole image CIN grades and the individual segment classifications by Dr. Frazier show variation in CIN grades. From Table 7.11 the image (“ouhsc_d8-2-cin3”) has inconclusive individual

segment classifications (“0”), where the CIN grades are given in four different CIN grading (0, 2, 3, 4). Three out of 10 segments are given a 4(CIN 3); however, the whole image classification by Dr. Frazier is 3 (CIN 2), which seems to be contradictory with what is discussed in the group where multi-levels (more than one) CIN stages exist. This illustrates the complexity of having varying local CIN information in the different segments and its impact on the whole image classification.

Using a more detailed analysis, the segments which are diagnosed as “4” in this group do not match the CIN 3 – segments which are shown in former groups. The size of nuclei is not as large and the color of the epithelium surface is not as dark either. They might be thought, to be CIN3, but to a very slight degree which means that the certain segments have just started to show a few characteristic feature of CIN 3.

Table 7.11. Whole image classification examples in which experts disagree and with multiple results within 10 segments.

Image Name	NLM Expert Classifications	Dr. Shelly Frazier Classifications		Cervical Intraepithelial Neoplasia grading scale 1 = Normal 2 = CIN 1 3 = CIN 2 4 = CIN 3	
ouhsc_d8-2-cin3	4	3			
					10 segments of one whole image, and the individual manual classification label from Dr. Frazier
0	3	3	4	2	
3	3	4	4	0	

Table 7.11. Whole image classification examples in which experts disagree and with multiple results within 10 segments. (Cont.)

Image Name	NLM Expert Classifications	Dr. Shelly Frazier Classifications		Cervical Intraepithelial Neoplasia grading scale 1 = Normal 2 = CIN 1 3 = CIN 2 4 = CIN 3	
ouhsc_d14-1-cin3	4	3			
		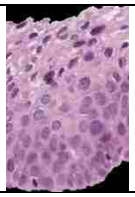			10 segments of one whole image, and the individual manual classification label from Dr. Frazier
4	4	3	3	3	
3	4	4	4	3	

Also from Table 7.11, the image “ouhsc_d14-1-cin3” has different expert whole image classifications, where one from Dr. Frazier is more conservative to be “3”(CIN 2) other than “4”(CIN 3) from Dr. Zuna. As it can be seen, in most of the 10 segments, dark nuclei are gathering around about the top half of the epithelium, but some light ones are in the bottom half, and considering all the classification of all the 10 segments, the “mid 4 images” are all diagnosed as “3”, which may be the reason why it is classified as CIN 2 that the mid-part segments contain the majority of convincing information that can be used for a reasonable CIN classification.

Overall, examining the CIN classifications for the 62 image data set and 620 segments, only 30 segments are given “0”, meaning that those segments exist without

enough useful information for CIN classification. Below follows the statistical diagram from the segment results of Dr. Frazier in Figure 7.3:

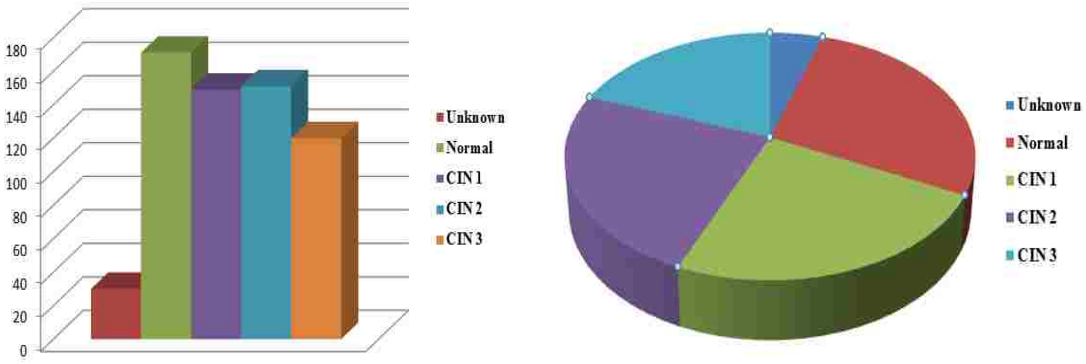

Figure 7.3. Distribution of different CIN grading scales over 620 segments.

According to the statistical information drawn from all the classification results, compared between two experts, it is known that Dr. Frazier's classification is more in detail; all of the 10 segments results of every image are classified; Meanwhile, Dr. Frazier's results tend to be more conservative in that they sometimes shows a lower CIN level or even "0" at the lack of enough information, while most of the final results for the whole images remain the same with the NLM expert's classifications.

Figure 7.4 shows the number of the individual segment results which match the final CIN classifications of those images. As observed, it is difficult to assess which segment takes a great advance in leading to the correct whole image CIN classification.

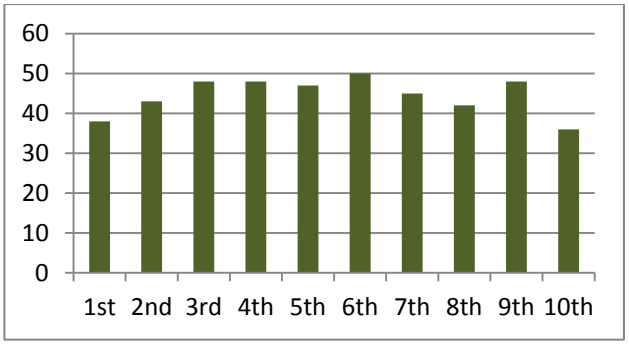

Figure 7.4. Distribution of individual segment classifications which match the whole image CIN classifications.

Figure 7.5 below shows the statistical result that the number of each segment which fits the final result for the whole image; and it is counted after eliminating the data from Section.7.1 (One same CIN stage for all the 10 segments of one whole image). As it is seen, generally, that the 6th and 9th segment match the most in comparison with the final classification; Meanwhile, the 1st, 8th and 10th segment have the worse matching accordingly.

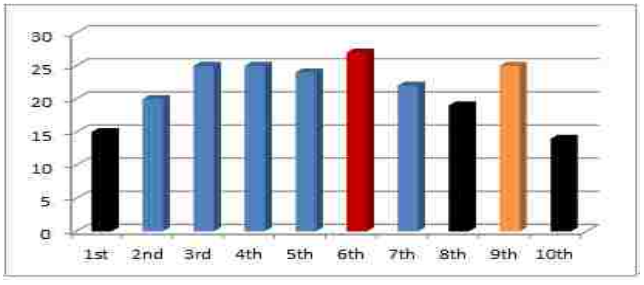

Figure 7.5. Distribution of individual segment classifications which match the whole image classifications where there is variation in the 10 individual segments within an image.

Figure 7.6 is obtained by eliminating "10 segments result distributed in 2 different levels" data from the former data, the 6th and 7th still remain high and the 3rd segment stands out in this result. And if a glance is given to the former two diagrams, it can be found that all the three segments (3rd, 6th, 7th) are relatively high-matching compared with the rest of the individual segments.

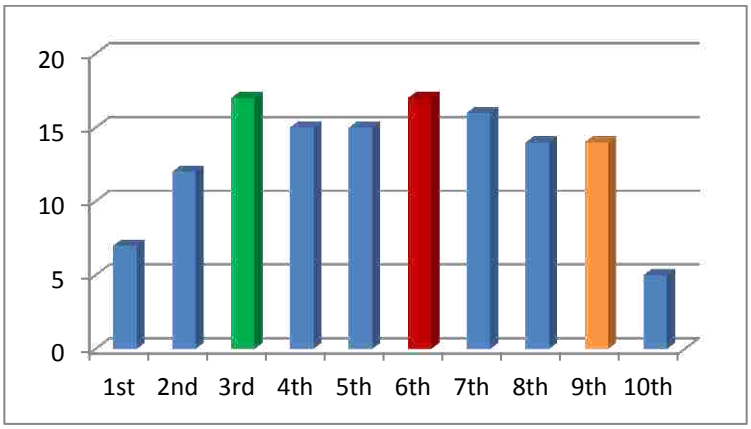

Figure 7.6. Distribution of segment results which match the final classification results (without all same results, and group with 2 different CIN levels).

There are 5 images in which the two experts differ in their CIN grade classifications. For all 5 images, the CIN classifications differ by a single grade. Accordingly, there are no significant variations in CIN grade classifications for the whole image for the two expert pathologists.

8. CONCLUSION

In this study, an automated CIN grade classification of vertical segmented epithelium regions is developed. The method developed includes medial axis determination, bounding box determination and partitioning the whole epithelium region into several vertical segments with the respect of medial axis. Then as many as 137 features are generated and taken all through experiment procedures which include leave-one out, normal vs. CIN, Normal+CIN1 vs. CIN2+3, off by one, and yield the final results through data fusion. And the features generated consist of texture, color, triangle, , nuclei, light area, combined features, layer-by-layer triangle features, and basal membrane features.

Experimental results from this study show higher CIN classification with 90.32% for exact label classification and 96.77% for normal vs. CIN classification compared to 70.5% and 90.2%, respectively, from previous research [8]. Some of the features in this study such as nuclei, light area, and layer-by-layer triangle features outperform other features and contribute a lot in improving the CIN classification, demonstrating the potential for vertical segmentation and the horizontal layer by layer analysis for enhancing CIN grading for the epithelium. Overall, most of the CIN grade assessments for the epithelium histology images from the two pathologists agree contribute to the similarity of automated CIN classification results reported in this thesis. The epithelium images which the pathologists disagree provide the basis for discovering different ways to fuse classification data for each single segment or a different method to update the weight in the neural network used in classification.

BIBLIOGRAPHY

[1] Parkin DM, Bray FI, Devesa SS. "Cancer burden in the year 2000," *The global picture*, Eur J Cancer 2001; 37 (Suppl. 8): S4-66

[2] Jeronimo J, Schiffman M. "A tool for collection of region based data from uterine cervix images for correlation of visual and clinical variables related to cervical neoplasia," *Proceedings of the 17th IEEE Symposium on Computer-Based Medical Systems*, 2004. pp. 558-62.

[3] Kumar V, Abbas A, Fausto N, Aster J. Robbins, "Cotran pathologic basis of disease. 8th ed. Philadelphia (PA)." *Saunders Elsevier*, 2009.

[4] He L, Long LR, Antani S, Thoma GR, "Computer assisted diagnosis in histo-pathology," *Sequence and genome analysis: methods and applications*, iConcept Press; 2001. P. 271-87.

[5] Wang Y, Crookes D, Eldin OS, Wang S, Hamilton P, Diamond J, "Assisted diagnosis of cervial intraepithelial neoplasia (CIN)," *IEEE J Sel Topics Signal Process*, 2009; 3(1): 112-21.

[6] McCluggage WG, "Inter- and intra-observer variation in the histopatho logical reporting of cervical squamous intraepithelial lesions using a modified Bethesda grading system," *BJOG: Int J Obstet Gynecol*, 1998; 105(2): 206-10.

[7] Ismail SM, Colclough AB, Dinnen JS, Eakins D, Evans DM, Gradwell E, O'Sullivan JP, Summerell JM, Newcombe R, "Reporting cervial intra-epithelial neoplasia agreement," *Histopathology*, 1990; 16(4): 371-6.

[8] Soumya De, R. Joe Stanley, Cheng Lu, Rodney Long, Sameer Antani, George Thoma, Rosemary Zuna, "A fusion-based approach for uterine cervical cancer histology image classification" *Computerized Medical Image and Graphics*, 2013;

[9] Maurer CR, Rensheng Q, Raghavan V, "A linear time algorithm for computing exact Euclidean distance transforms of binary images in arbitrary dimensions," *IEEE Trans Pattern Anal Mach Intell*, 2003;25(2):265–70.

[10] Price GJ, Mccluggage WG, Morrison ML, Mcclean G, Venkatraman L, Diamond J, Bharucha H, Montironi R, Bartels PH, Thompson D, Hamilton PW, "Computerized diagnostic decision support system for the classification of preinvasive cervical squamous lesions" *Hum Pathol*, 2003;34(11):1193–203.

[11] Cheng Lu. "Uterine cervical cancer histology image feature extraction and classification," 2013;

[12] Soumya De, “Data Fusion Techniques for Structural Health Monitoring and Signal Integrity Applications,” 2012

[13] Preparata FR, Shamos MI, “Computational geometry: an introduction,” *New York: Springer-Verlag*, 1985.

VITA

Peng Guo was born in city of Jilin in the province of Jilin, China in 1989. He did his schooling at the Tianjin Road Elementary School (1996-2002), 7th Middle School (2002-2005), in Jilin, and No.1 Middle School (2005-2008) before going to Northeast Electrical University in his hometown, for his Bachelor of Science degree in Electrical Engineering from the Department of Automation (2012). In July of the same year, he entered Missouri University of Science and Technology, where he is expected to receive his Master of Science degree in Electrical Engineering from the Department of Electrical and Computer Engineering in 2014.